

# Numerical study of quantum many body systems

*Haoran Hu*

Department of Physics, Southeast University, Nanjing, China, 210096

213210160@seu.edu.cn

---

**Abstract.** This paper explores the numerical study of quantum many-body systems with an emphasis on exact diagonalization techniques. The complexity of strongly correlated systems, often governed by large Hilbert spaces, presents significant computational challenges, making exact solutions difficult. In this work, we examine methods to simplify these systems by leveraging techniques such as the Schrieffer-Wolff transformation, which decouples high-energy and low-energy states, and the use of symmetry operators to block-diagonalize Hamiltonians and so on. These approaches are demonstrated with examples such as the hydrogen atom and a lambda system. The second part of the paper focuses on specific case studies, including a one-dimensional spin model and Bose-Hubbard model. The latter is crucial for understanding the behavior of interacting bosons in lattice systems and phenomena such as the superfluid-Mott insulator transition. We present a detailed investigation of the phase diagram for the one-dimensional Bose-Hubbard model using both exact diagonalization and mean field theory, providing insights into its quantum phase transitions. This study underscores the potential of exact diagonalization in quantum simulations and highlights its relevance for experimental setups involving trapped ions and superconducting qubits.

**Keywords:** quantum simulation, exact diagonalization, Bose-Hubbard model, Schrieffer-Wolff transformation, effective Hamiltonian, Heisenberg model

---

## 1. Introduction

In recent years, significant experimental and theoretical advances have been made in the field of quantum many-body systems, driven by the quest to understand and manipulate strongly correlated states [1]. These states play a crucial role in various physical phenomena and hold promise for applications such as quantum computing [2] and quantum materials [3][4][5]. However, the inherent complexity of strongly correlated systems often presents substantial challenges, particularly in their large Hilbert space which made exact calculation of the intractable. In addition to the the recent development of numerical algorithms, such as tensor network or DMRG, which posed assumptions to the many body system, we still wish to apply exact treatment to many body systems for the purpose of quantum simulation of strongly correlated systems in table top experiments, such as trapped ions, neutral atoms or superconducting qubits. The project is organized to: 1. study the basic techniques of exact diagonalization of quantum many body systems and 2. learn how this can be applied to models frequently used in quantum simulation, such as Bose Hubbard model.

The first part of this paper focuses on the essential prerequisites for exact diagonalization. We begin with a detailed examination of the Schrieffer-Wolff (SW) transformation [6], using a lambda system as an illustrative example. This transformation is pivotal in reducing the complexity of the Hamiltonian by decoupling high-energy and low-energy states. Additionally, we explore the concepts of symmetries and symmetry operators, demonstrating their applications with the hydrogen atom. By exploiting the inherent symmetries of a system, we can simplify

Hamiltonians to block-diagonal forms that are more manageable for exact studies.

The second part of the paper explores specific case studies of quantum many-body systems. We begin by examining a one-dimensional spin model, with a focus on the degeneracy of the ground state energy and the process of block diagonalization. This model is crucial for understanding how symmetry considerations can expedite the exact diagonalization process.

Following this, we analyze the Bose-Hubbard model, which is key to describing the behavior of interacting bosons on a lattice and offers insights into phenomena such as the superfluid-Mott insulator transition in ultracold atomic systems. Specifically, we investigate the phase diagram of the 1D Bose-Hubbard model using both exact diagonalization and mean field theory.

## 2. Prerequisite to the study of quantum many body system

In the study of complex multilevel systems, such as atoms or molecules, leveraging symmetries to reduce the Hilbert space dimension is a fundamental step. Beyond this initial reduction, it is often possible to further isolate a subset of states that are only weakly and non-resonantly coupled to the rest of the system. The dynamics of this subset can then be approximated by a Hamiltonian of reduced dimensionality. In this reduced Hamiltonian, the influence of interactions with states outside the relevant subspace is incorporated through additive energy shifts and modified couplings.

### 2.1. Schrieffer Wolff transformation and Effective Hamiltonian

Schrieffer Wolff transformation is a basic method to get the low energy dynamics from the full Hamiltonian. This method is broadly used in many body systems [7][8][9]. t-J model can be derived from Hubbard model through Schrieffer Wolff transformation [9], explaining the superconductivity mechanism in high temperature superconductors of copper oxides. In the Fermi-Hubbard model, virtual doublon-hole excitations play a crucial role in mediating antiferromagnetic spin-exchange interactions within the effective model, often referred to as the t-J-3s model [10]. Formally this procedure is described by performing a unitary Schrieffer-Wolff basis transformation. It is the broad use of SW transformation method in strong correlated system. The Schrieffer-Wolff transformation is a perturbative method used to simplify the Hamiltonian of a quantum system by eliminating certain off-resonant couplings, thereby focusing on the essential low-energy dynamics. This technique involves a unitary transformation that decouples the high-energy and low-energy subspaces of the system. The transformed Hamiltonian, known as the effective Hamiltonian, captures the low-energy behavior while disregarding the high-energy excitations. Suppose that the total Hamiltonian contains many-body interactions, perturbation theory allows one to construct a simpler high energy simulator Hamiltonian with only two-body interactions whose low-energy properties (such as the ground state energy) approximate the total Hamiltonian. Therefore, in many papers, SW transformation is used with perturbation theory [11][12]. Mathematically, the SW transformation is represented as:

$$H_{eff} = e^S H e^{-S} \tag{1}$$

where H is the original Hamiltonian, and S is an anti-Hermitian operator chosen such that the transformed  $H_{eff}$  eliminates or reduces the coupling between the low-energy and high-energy states.

#### 2.1.1. Lambda system

Over the past few decades, advancements in atomic, molecular, and optical (AMO) technology have significantly enhanced our ability to study and simulate strongly correlated quantum systems. One of the most common and fundamental models in AMO physics is the lambda system, which consists of three energy levels where two lower levels are connected to an excited state via optical transitions. The scheme is shown in the figure 1, which is ubiquitous in atomic physics.

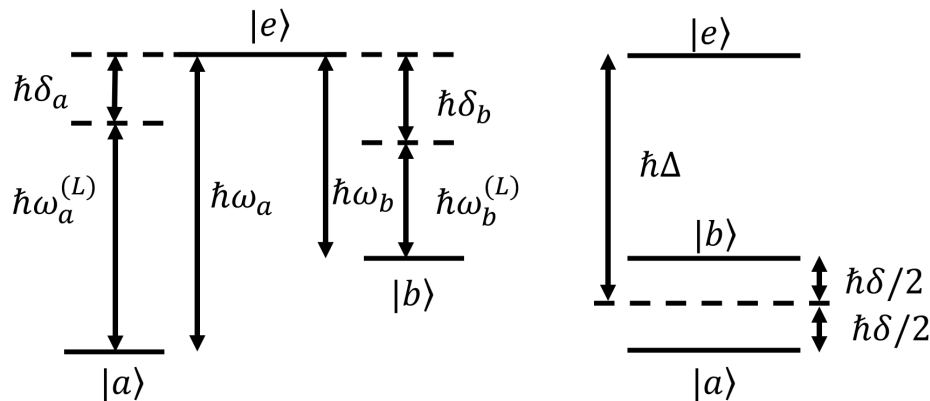


Figure 1: lambda system's level scheme

It consists of two lower states  $|a\rangle, |b\rangle$  coupled to an excited level  $|e\rangle$  via two off-resonance lasers: the detunings are denoted  $\delta_k = \omega_k - \omega_k^{(L)}$  ( $k = a, b$ ), where  $\hbar\omega_k = E_e - E_k$  and  $\omega_{a,b}^{(L)}$  are the frequencies of the lasers. In this system,  $|a\rangle - > |b\rangle$  is the forbidden transition. We need to use one laser to excite electrons from  $|a\rangle$  to  $|e\rangle$  and another laser to deexcite electrons from  $|e\rangle$  to  $|b\rangle$ . In order to make more electrons to excite to  $|b\rangle$  instead of staying at  $|e\rangle$ , we can excite  $|a\rangle$  into a virtual state (dotted line in the figure 1) and then deexcite electrons to  $|b\rangle$ . The energy difference between virtual state and  $|e\rangle$  is small. We can write the Hamiltonian  $H = H_0 + V$ , where  $H_0$  is the unperturbed Hamiltonian of this system which is independent of time and  $V$  is the interaction potential between lasers and atoms. If we choose the middle of  $|a\rangle$  and  $|b\rangle$  as zero potential. Then  $H_0 = \hbar(\Delta - \omega_a) |a\rangle \langle a| + \hbar(\Delta - \omega_b) |b\rangle \langle b| + \hbar\Delta |e\rangle \langle e|$ . In the electromagnetic wave, electric field is much larger than magnetic field. So that we only consider the interaction between electric field and atoms. We see atoms as dipoles  $\vec{d}$  which have the energy  $-\vec{d} \cdot \vec{E}$  in the electric field. We write the electric field as  $\vec{E}(\vec{r}, t) = \vec{E}_a \cos(\vec{k}_a \cdot \vec{r} - \omega_a^{(L)} t) + \vec{E}_b \cos(\vec{k}_b \cdot \vec{r} - \omega_b^{(L)} t)$ . Because the wavelength of electric field is much larger than the interatomic distance, it is a uniform electric field in the atomic scale. Then the electric field becomes:

$$\begin{aligned} \vec{E}(t) &= \vec{E}_a \cos(\omega_a^{(L)} t) + \vec{E}_b \cos(\omega_b^{(L)} t) \\ &= E^+ + E^- \end{aligned} \quad (2)$$

where  $E^+ = \frac{1}{2}(\vec{E}_a e^{-i\omega_a^{(L)} t} + \vec{E}_b e^{-i\omega_b^{(L)} t})$  and  $E^- = \frac{1}{2}(\vec{E}_a e^{i\omega_a^{(L)} t} + \vec{E}_b e^{i\omega_b^{(L)} t})$ .  $\vec{E}_a$  only functions on  $|e\rangle$  and  $|a\rangle$  and  $\vec{E}_b$  only functions on  $|e\rangle$  and  $|b\rangle$ . The electric dipole can be expressed as:

$$\vec{d} = I \vec{d} I = (|a\rangle \langle a| + |b\rangle \langle b| + |e\rangle \langle e|) \vec{d} (|a\rangle \langle a| + |b\rangle \langle b| + |e\rangle \langle e|) \quad (3)$$

where  $|a\rangle, |b\rangle, |e\rangle$  spans a space and  $I$  is the Identity matrix. Due to the transition prohibition between  $|a\rangle$  and  $|b\rangle$  and  $\langle i | \vec{d} | i \rangle = 0$ , where  $i = a, b, e$  (the integral of odd function in the symmetric space is 0). The dipole becomes:

$$\begin{aligned} \vec{d} &= (d_{ae}^+ \sigma_1 + d_{be}^+ \sigma_2) + (d_{ae}^- \sigma_1^\dagger + d_{be}^- \sigma_2^\dagger) \\ &= \vec{d}^+ + \vec{d}^- \end{aligned} \quad (4)$$

where  $\sigma_1 = |a\rangle \langle e|, \sigma_2 = |b\rangle \langle e|, d_{ae}^+ = \langle a | \vec{d} | e \rangle, d_{be}^+ = \langle b | \vec{d} | e \rangle$ . The interaction term can be expressed as:

$$V = -\vec{d} \cdot \vec{E} \quad (5)$$

Remembering that  $E_a$  only acts on  $|a\rangle$  and  $E_b$  only acts on  $|b\rangle$ , we define  $\Omega_i = -\frac{\langle e | \vec{d} \cdot \vec{E}_i | i \rangle}{\hbar}, i = a, b$ . Then we put  $V$  in the interaction picture.

$$V_I = e^{\frac{i}{\hbar} H_0 t} V e^{-\frac{i}{\hbar} H_0 t} \quad (6)$$

After Schrieffer Wolff (SW) transformation and Rotating Wave Approximation (RWA), the interaction term becomes:

$$V_I = \left( \frac{\hbar\Omega_a^*}{2} e^{it(\omega_a - \omega_a^{(L)})} \sigma_1^\dagger + \frac{\hbar\Omega_b^*}{2} e^{it(\omega_b - \omega_b^{(L)})} \sigma_2^\dagger \right) + \left( \frac{\hbar\Omega_a}{2} e^{-it(\omega_a - \omega_a^{(L)})} \sigma_1 + \frac{\hbar\Omega_b}{2} e^{-it(\omega_b - \omega_b^{(L)})} \sigma_2 \right) \quad (7)$$

We change the interaction term into the Schrodinger picture after throwing away fast rotating term.

$$\hat{V} = \hbar \begin{pmatrix} 0 & 0 & \frac{\Omega_a^*}{2} e^{i\omega_a^{(L)} t} \\ 0 & 0 & \frac{\Omega_b^*}{2} e^{i\omega_b^{(L)} t} \\ \frac{\Omega_a}{2} e^{-i\omega_a^{(L)} t} & \frac{\Omega_b}{2} e^{-i\omega_b^{(L)} t} & 0 \end{pmatrix} \quad (8)$$

Then the total Hamiltonian becomes:

$$\hat{H} = \hat{H}_0 + \hat{V} = \hbar \begin{pmatrix} \Delta - \omega_a & 0 & \frac{\Omega_a^*}{2} e^{i\omega_a^{(L)} t} \\ 0 & \Delta - \omega_b & \frac{\Omega_b^*}{2} e^{i\omega_b^{(L)} t} \\ \frac{\Omega_a}{2} e^{-i\omega_a^{(L)} t} & \frac{\Omega_b}{2} e^{-i\omega_b^{(L)} t} & \Delta \end{pmatrix} \quad (9)$$

This Hamiltonian is hard to solve and we can do a rotation transformation to apply this Hamiltonian into the rotating coordinate system. Then the final Hamiltonian becomes:

$$H = \hbar \begin{pmatrix} \Delta - \omega_a + \omega_a^{(L)} & 0 & \frac{\Omega_a^*}{2} \\ 0 & \Delta - \omega_b + \omega_b^{(L)} & \frac{\Omega_b^*}{2} \\ \frac{\Omega_a}{2} & \frac{\Omega_b}{2} & \Delta \end{pmatrix} = \hbar \begin{pmatrix} -\frac{\delta}{2} & 0 & \frac{\Omega_a^*}{2} \\ 0 & \frac{\delta}{2} & \frac{\Omega_b^*}{2} \\ \frac{\Omega_a}{2} & \frac{\Omega_b}{2} & \Delta \end{pmatrix} \quad (10)$$

It is the same as in the paper [13]. By using RMA and SW transformation, we simplify a complex, unsolvable Hamiltonian to a Hamiltonian like equation (10).

## 2.2. Symmetries and symmetry operators

Although we obtain the low-energy effective Hamiltonian from the Schrieffer-Wolff (SW) transformation, solving this Hamiltonian remains challenging. To simplify the problem, we can exploit symmetries within the Hamiltonian. If we have a symmetry operator  $\hat{P}_R$  under which the Hamiltonian is invariant, this operator commutes with the Hamiltonian. Moreover, if  $\hat{P}_R$  is a Hermitian operator, then  $\hat{H}$  and  $\hat{P}_R$  can be block diagonalized.

It is clear that these operators form a group. If an operator  $\hat{P}_R$  belongs to this group, its inverse  $\hat{P}_R^{-1}$  must also be in the group. Additionally, the product of two operators within the group remains an operator of the group, as they can be considered as acting independently on the Hamiltonian. The associative property is evidently satisfied, which ensures the group structure. Regardless of whether the operators  $\hat{P}_R$  correspond to rotations, reflections, translations, or permutations, these symmetry operations do not affect the eigenvalues of the Hamiltonian. If the action of  $\hat{P}_R$  on an arbitrary vector composed of  $l$  eigenfunctions yields an  $l \times l$  matrix representation of  $\hat{P}_R$  in block diagonal form, the matrix is block-diagonalized into smaller blocks, just like showing in the figure 2. We can then isolate each block and calculate its eigenvalues, significantly simplifying the overall calculation. For instance, using a symmetry operator, we can block-diagonalize a  $7 \times 7$  matrix into the direct sum of a  $3 \times 3$  matrix and a  $4 \times 4$  matrix. Consequently, instead of calculating the eigenvalues of a  $7 \times 7$  matrix, we only need to compute the eigenvalues of the smaller  $3 \times 3$  and  $4 \times 4$  matrices.

$$[\hat{H}, \hat{P}_R] = 0 \quad \hat{H}: \text{Hamiltonian}, \hat{P}_R: \text{symmetry operator}$$

$$\hat{S}^\dagger \hat{P}_R \hat{S} \Rightarrow \begin{pmatrix} \lambda_1 & 0 & 0 & 0 & & & \\ 0 & \lambda_1 & 0 & 0 & \dots & & 0 \\ 0 & 0 & \lambda_2 & 0 & & & \\ 0 & 0 & 0 & \lambda_2 & & & \\ \vdots & & & & \ddots & & \\ & & & & & \lambda_n & 0 & 0 \\ 0 & & & & & 0 & \lambda_n & 0 \\ & & & & & 0 & 0 & \lambda_n \end{pmatrix}, \lambda_1, \lambda_2 \dots \lambda_n \text{ is the eigenvalue of } \hat{P}_R$$

$$\hat{S}^\dagger \hat{H} \hat{S} \Rightarrow \begin{pmatrix} \square & 0 & 0 & & & & \\ & 0 & 0 & \dots & & & 0 \\ 0 & 0 & \square & & & & \\ 0 & 0 & & \ddots & & & \\ \vdots & & & & \ddots & & \\ & & & & & \square & \\ 0 & & & & & & \square \end{pmatrix} \quad \leftarrow \text{Block Diagonalized}$$

Figure 2: The hamiltonian is block diagonalized under symmetry operators

### 2.2.1. SO(4) in hydrogen atom

The hydrogen atom is a prime example of how symmetry operators can be used to analyze a system. The Hamiltonian of the hydrogen atom is invariant under rotational transformations, making it natural to introduce the SO(3) symmetry group into this system. The dimension of the irreducible representation of SO(3) is  $2l + 1$ , which corresponds to the degeneracy of energy levels. However, according to the Schrödinger equation, when the principal quantum number  $n$  is determined,  $l$  can take values from 0 to  $n - 1$ . The actual degeneracy of energy levels is  $\sum_{l=0}^{n-1} (2l + 1) = n^2$ , which is greater than  $2l + 1$ . In other words, the SO(3) group does not fully describe the degeneracy (or symmetry) of the hydrogen atom system.

To resolve this, we can show that the hydrogen atom actually possesses SO(4) symmetry. According to central field theory, this system has a Runge-Lenz vector defined as  $\mathbf{M} = \frac{1}{2m}(\mathbf{p} \times \mathbf{L} - \mathbf{L} \times \mathbf{p}) - \frac{e^2}{r} \hat{\mathbf{r}}$ , which can also be expressed as  $\mathbf{M} = \frac{1}{m}(\mathbf{p} \times \mathbf{L} - i\hbar\mathbf{p}) - \frac{e^2}{r} \hat{\mathbf{r}}$ . We can prove that  $[H, \mathbf{M}] = 0$ , indicating that  $\mathbf{M}$  is conserved.

Here,  $\mathbf{L}$  is the generator of SO(3), and  $\mathbf{M}$  acts as another generator of SO(3). However, unlike  $\mathbf{L}$ ,  $\mathbf{M}$  does not satisfy the standard commutation relations of angular momentum. It satisfies:

$$[M_i, M_j] = -i\hbar\epsilon_{ijk} \frac{2H}{m} L_k \tag{11}$$

When we consider the bound state of hydrogen atoms, we can define  $\mathbf{N} = \sqrt{-\frac{m}{2E}}\mathbf{M}$ . We have below relations:

$$\begin{aligned} [L_i, L_j] &= i\hbar\epsilon_{ijk}L_k \\ [N_i, L_j] &= i\hbar\epsilon_{ijk}N_k \\ [N_i, N_j] &= i\hbar\epsilon_{ijk}L_k \end{aligned} \quad (12)$$

We now define  $\mathbf{I} = \frac{\mathbf{L}+\mathbf{N}}{2}$ ,  $\mathbf{K} = \frac{\mathbf{L}-\mathbf{N}}{2}$ .

$$\begin{aligned} \mathbf{I}^2 - \mathbf{K}^2 &= \frac{\mathbf{N} \cdot \mathbf{L} + \mathbf{L} \cdot \mathbf{N}}{2} = 0 \\ \mathbf{I}^2 + \mathbf{K}^2 &= \frac{\mathbf{N}^2 + \mathbf{L}^2}{2} = \frac{1}{2}(\mathbf{L}^2 - \frac{m}{2E}\mathbf{M}^2) = \frac{1}{2}(-\hbar^2 - \frac{m}{2E}e^4) \end{aligned} \quad (13)$$

Let the eigenvalues of  $\mathbf{I}^2$  and  $\mathbf{K}^2$  be  $i(i+1)\hbar^2$  and  $k(k+1)\hbar^2$ , respectively. From equation (13), we obtain  $i = k$  and  $E = -\frac{me^4}{2\hbar^2(2k+1)^2}$ . This result indicates that only the representation of SO(4) satisfying  $I = K$  correctly describes the bound energy levels of the hydrogen atom.

Furthermore, we can choose a matrix representation of the SO(4) group. Since  $\mathbf{M}$  is a symmetry operator of this system, we can apply the numerical method illustrated in Figure 2 to calculate the energy levels of the hydrogen atom in matrix form.

### 3. Case study of quantum many body systems

Many one-dimensional (1D) spin models are exactly solvable, making them highly valuable for theoretical studies. For example, the 1D Ising model, the Heisenberg model, and the XY model all have known solutions. The two-dimensional Ising model was exactly solved by Lars Onsager in 1944[14]. However, solving models in higher dimensions is generally much more challenging.

One-dimensional spin models, on the other hand, can be analyzed in detail using various methods, such as the Bethe Ansatz, matrix product states, and quantum field theory. Therefore, 1D spin models are an excellent choice for studying strongly correlated systems. In this paper, we focus on two typical 1D models. As discussed in the previous section, we can use the Schrieffer-Wolff (SW) transformation and symmetries to simplify our calculations. These methods allow us to perform numerical calculations for certain Hamiltonians.

#### 3.1. Exact Diagonalization of 1D spin model

In 1D spin model, Heisenberg model is one of the most famous one. First, we consider a six-particle Heisenberg chain which can be written as follows:

$$\hat{H} = \sum_{\langle i,j \rangle=1}^6 S_{ix}S_{jx} + \lambda_1 S_{iy}S_{jy} + \lambda_2 S_{iz}S_{jz} \quad (14)$$

This Hamiltonian satisfies the periodic boundary condition and  $\lambda_1, \lambda_2$  are two variables. We can rewrite this Hamiltonian into the form of spin-up operator  $S_i^+ = S_{ix} + iS_{iy}$  and spin-down operator  $S_i^- = S_{ix} - iS_{iy}$ .

$$\hat{H} = \sum_{\langle i,j \rangle} \frac{1-\lambda_1}{4} (S_i^+ S_j^+ + S_i^- S_j^-) + \frac{1+\lambda_1}{4} (S_i^- S_j^+ + S_i^+ S_j^-) + \lambda_2 S_{iz} S_{jz} \quad (15)$$

Naturally, if a particle at a site has spin-up, we label it as 1; otherwise, we label it as 0. For example, if the spins of six particles are up, up, down, down, up, down, we represent this configuration as  $|110010\rangle$ . We then use these basis states to construct the matrix form of the Hamiltonian. Note the following actions of the spin operators:  $S_i^+ |\dots 1\dots\rangle = 0$ ,  $S_i^+ |\dots 0\dots\rangle = |\dots 1\dots\rangle$ ,  $S_i^- |\dots 1\dots\rangle = |\dots 0\dots\rangle$ ,  $S_i^- |\dots 0\dots\rangle = 0$ ,  $S_{iz} |\dots 1\dots\rangle = \frac{1}{2} |\dots 1\dots\rangle$ , and  $S_{iz} |\dots 0\dots\rangle = -\frac{1}{2} |\dots 0\dots\rangle$ .

We can use a symmetry operator to block diagonalize the Hamiltonian, simplifying our calculations. Specifically, for this system, the Hamiltonian is invariant under rotation, meaning that the rotation operator is a symmetry operator and commutes with the Hamiltonian. When the symmetry operator is diagonalized in a new basis, the Hamiltonian will also be block diagonalized in that same basis. Therefore, we can use the eigenvectors of the symmetry operator to achieve a block diagonalization of the Hamiltonian.

##### 3.1.1. Symmetry operators in 1D spin model

- **Spin Flip Operator** When the spin flip operator is applied to a basis state, it flips the spin of each particle: spin-up changes to spin-down, and spin-down changes to spin-up (where 0 represents the spin-down state and 1 represents the spin-up state). It is clear that this operator is a symmetry operator. For example, if the initial state is  $|110010\rangle$ , applying the spin flip operator  $S$  transforms it to the state  $|001101\rangle$ . When this operator  $S$  is applied twice, the system returns to the initial state. Thus, the operator has two eigenvalues, 1 and -1.

- **Parity Operator** The parity operator, when applied to a basis state, swaps the positions of particles symmetrically. Specifically, the particle at site 1 is swapped with the particle at site 5, the particle at site 2 is swapped with the particle at site 4, and the particles at sites 3 and 6 remain unchanged. If we visualize these 6 particles arranged in a circle, the line from particle 3 to particle 6 acts as a reflection mirror. Due to the periodic boundary conditions, this operator is also a symmetry operator. For example, if the initial state is  $|110010\rangle$ , applying the parity operator  $P$  results in the state  $|100110\rangle$ . Applying  $P$  twice returns the system to the initial state. Therefore, the parity operator has two eigenvalues, 1 and -1.
- **Rotation Operator** The rotation operator can be constructed to cyclically exchange particles between adjacent sites. For instance, the particle at site 1 moves to site 2, the particle at site 2 moves to site 3, and so on. For example, if the initial state is  $|110010\rangle$ , applying the rotation operator  $R$  results in the state  $|011001\rangle$ . When this rotation operator  $R$  is applied six times, the system returns to the initial state, so  $R^6 = 1$ . The operator has six eigenvalues:  $1, e^{i\frac{\pi}{3}}, e^{i\frac{2\pi}{3}}, -1, e^{i\frac{4\pi}{3}},$  and  $e^{i\frac{5\pi}{3}}$ . These six eigenvalues correspond to rotations by angles of  $0, \frac{\pi}{3}, \frac{2\pi}{3}, \pi, \frac{4\pi}{3},$  and  $\frac{5\pi}{3}$ , respectively.

### 3.1.2. Block diagonalized Hamiltonian for 6 sites

After applying the spin flip operator, the Hamiltonian separates into two parts. Each part is represented by a 32x32 matrix, corresponding to the eigenvalues of the spin flip operator, -1 and 1, respectively. The detailed values of these matrices can be found in the Appendix. Next, we apply the parity operator to the Hamiltonian in this new basis. Each 32x32 block is further block diagonalized into two smaller parts: a 12x12 block and a 20x20 block, representing the eigenvalues of the parity operator, -1 and 1, respectively.

We then proceed by applying the rotation operator. For the case of 6 sites, the eigenvalues of the rotation operator are  $1, -1, -\frac{1}{2},$  and  $\frac{1}{2}$  after the spin flip and parity operators have been applied. Notably, the eigenvalues  $-\frac{1}{2}$  and  $\frac{1}{2}$  exhibit a two-fold degeneracy. This degeneracy arises because rotations by angles of  $\frac{\pi}{3}$  and  $\frac{4\pi}{3}$ , as well as  $\frac{2\pi}{3}$  and  $\frac{5\pi}{3}$ , are equivalent in the new basis, leading to this two-fold degeneracy.

The final block-diagonalized Hamiltonian takes the form in the figure 3:

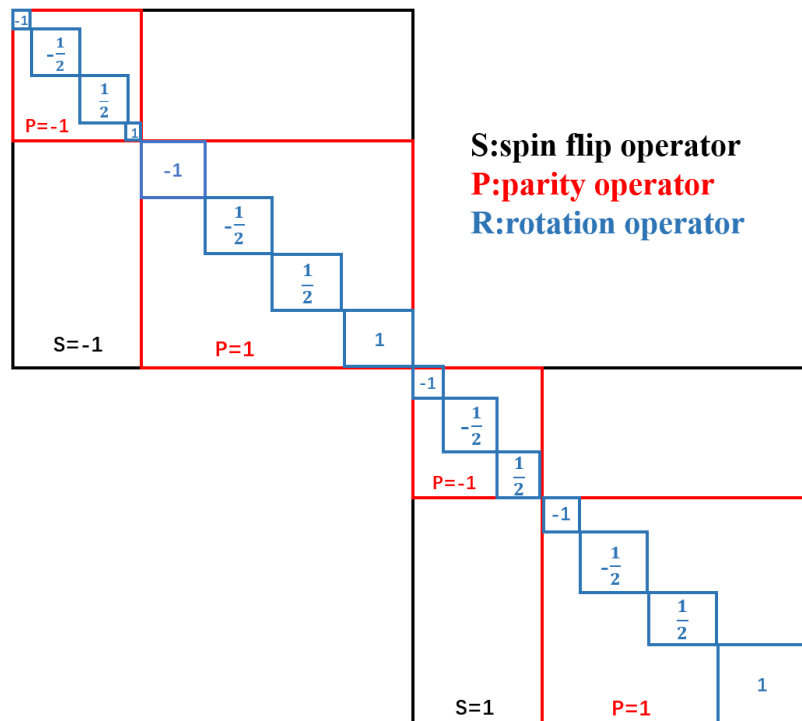


Figure 3: This is 6 particle block diagonalized Hamiltonian after using spin flip operator, parity operator and rotation operator. Each block in this Hamiltonian has physical meaning. The lowest left block means this block has spin flip symmetry (S=1), parity symmetry (P=1), rotation symmetry (R=1).

Then we can easily calculate the eigenvalue of each block and find the ground energy. To make it more clear, we plot ground energy vs  $\lambda_1$  for different  $\lambda_2$  graph.

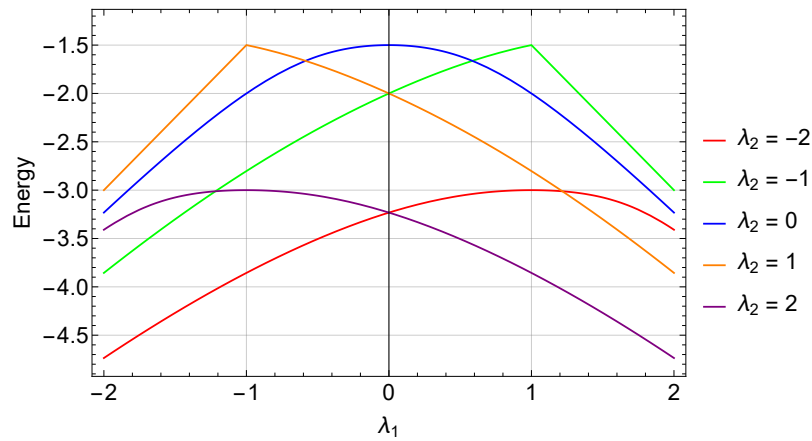


Figure 4: Theoretical ground energy for 1D spin model

In the figure 4, we observe that when we select  $\lambda_2$  and its inverse, their graphs are symmetric about the y-axis. This symmetry is expected. Since we can arbitrarily choose the spin operators  $S_y$  and  $S_z$ ,  $\lambda_1$  and  $\lambda_2$  can be interchanged in the context of the Hamiltonian. Consequently, when we fix  $\lambda_2$  and plot the energy as a function of  $\lambda_1$ , we obtain the same result.

### 3.1.3. Properties of ground energy

To find the ground energy properties, 6 sites are not enough. We gradually increase site numbers just as shown in the figure 5.

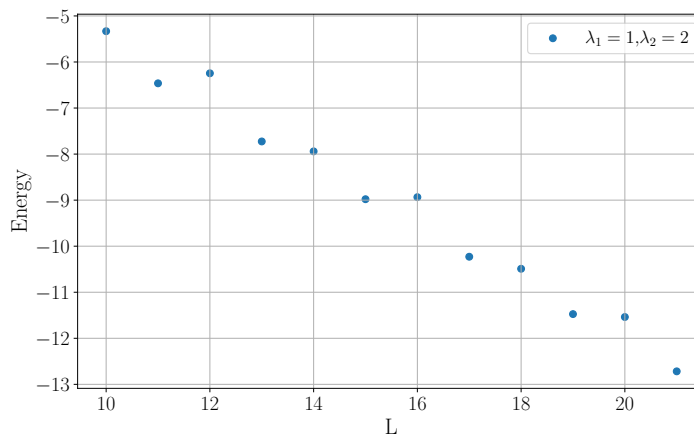


Figure 5: Ground energy for different sizes[15]

As size goes bigger, which means closer to actual situation, we find that the ground energy becomes lower and lower because of more spins in the system.

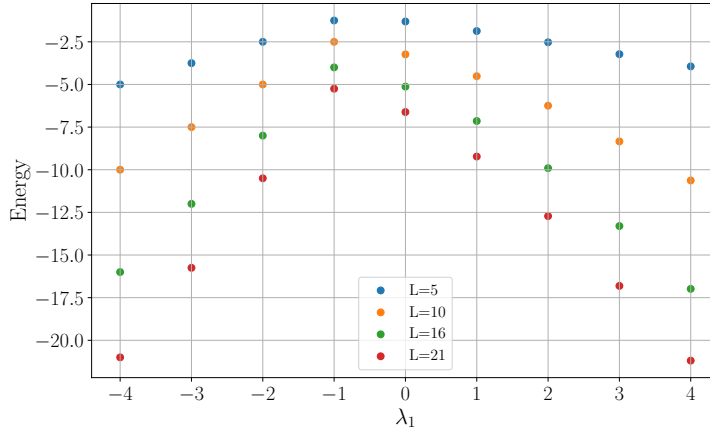


Figure 6: Ground energy for different  $\lambda_1$  when  $\lambda_2 = 1$  [15]

In the figure 6, as  $\lambda_2$  increases and  $\lambda_1$  becomes larger, the ground energy decreases continuously. This implies that when the spin preferentially aligns in a particular direction, it becomes easier for the spin to rotate into that direction, leading to a lower energy state. Moreover, as  $\lambda_2$  increases, the ground energy also decreases. This can be demonstrated by considering operators in other directions as perturbations. The resulting Hamiltonian is given by:

$$\hat{H} = \lambda_2 \sum_{i=1}^N S_{iz} S_{(i+1)z} \tag{16}$$

Therefore, as  $\lambda_2$  increases, the lowest eigenstate tends to approach  $|000000\rangle$  for 6 sites, which corresponds to the lowest energy of  $-3\lambda_2$ . Conversely, when  $\lambda_2$  is sufficiently small, the ground state becomes  $|111111\rangle$  for 6 sites. This indicates the existence of a state with a maximum ground energy. As shown in Fig. 4, the maximum ground energy occurs when  $\lambda_2 \approx \pm 1$ . Additionally, it is evident that as the number of sites increases (bringing the system closer to realistic conditions),  $\lambda_2$  is more likely to be around  $\pm 1$ .

### 3.1.4. Properties of $S_z$

Then we want to find the mean value of  $\sum_{i=1}^N S_{iz}$ .

$$\langle \sum_{i=1}^N S_{iz} \rangle = \langle \psi | \sum_{i=1}^N S_{iz} | \psi \rangle \tag{17}$$

where  $\psi$  is the ground state of the hamiltonian. First, we set  $\lambda_1$  unchanged and plot  $S_z$  versus  $\lambda_2$ .

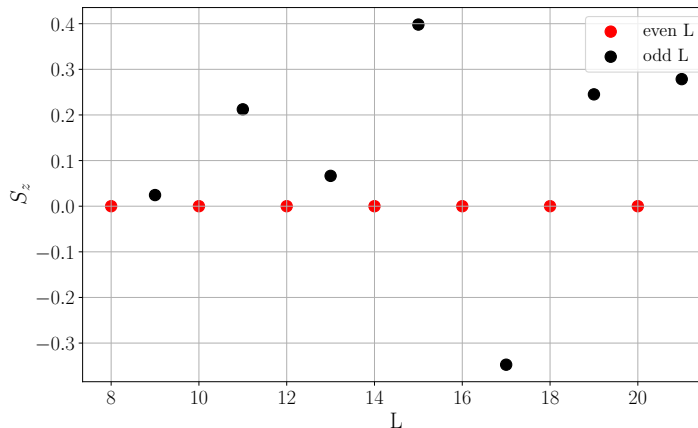
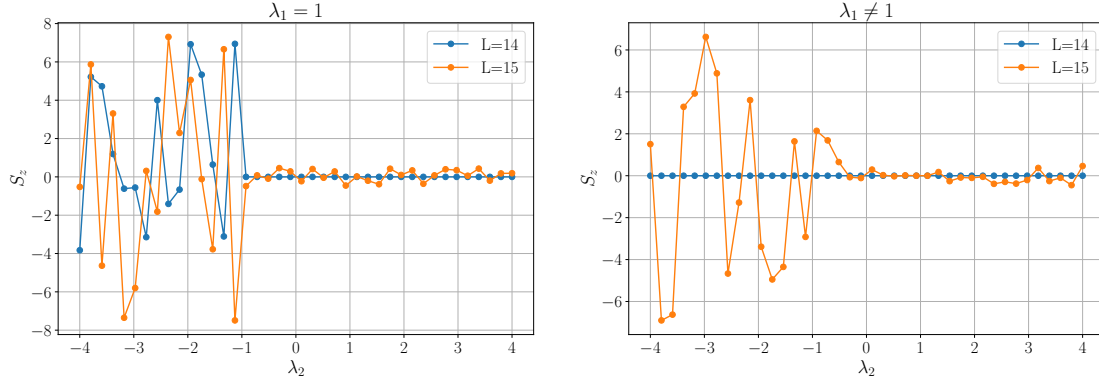


Figure 7:  $S_z$  for different sizes when  $\lambda_1 = 2$  and  $\lambda_2 = 1$ [15]


 Figure 8:  $S_z$  for different  $\lambda_2$  when  $\lambda_1$  has different values[15]

In the figure 7, we find that for even numbers of sites,  $S_z$  is zero. However, for odd numbers of sites,  $S_z$  oscillates with  $\lambda_2$ . Moreover, as  $\lambda_2$  becomes greater than -1, the amplitude of this oscillation decreases. This indicates that for even numbers of sites, there is no net magnetic moment in the system. This generally implies that the spins are antiparallel, which is a more stable configuration.

Due to symmetry breaking or local spin asymmetry, a non-zero expectation value of  $S_z$  may appear in the ground state. This phenomenon reflects a local spin bias or asymmetry in the system. This behavior is observed when  $\lambda_1 \neq 1$ .

However, when  $\lambda_1 = 1$ , the situation changes. For  $\lambda_1 = 1$ ,  $S_z$  oscillates with  $\lambda_2$  regardless of whether the number of sites is odd or even. For even numbers of sites and  $\lambda_2 > -1$ ,  $S_z$  remains zero. For odd numbers of sites and  $\lambda_2 > -1$ ,  $S_z$  oscillates with a smaller amplitude, just as shown in the figure 8.

### 3.1.5. Degeneracy of the ground energy

As discussed above, -1 and 1 are two significant values. Additionally, parity also influences the system. Therefore, when determining the degeneracy of the ground state, it is important to take these factors into account carefully.

Table 1: Ground energy degeneracy for even sites

	$\lambda_1 < -1$	$\lambda_1 = -1$	$-1 < \lambda_1 < 1$		$\lambda_1 = 1$	$\lambda_1 > 1$
$\lambda_2 < -1$	1	1	$\lambda_1 = -\lambda_2$	$\lambda_1 \neq -\lambda_2$	2	1
$\lambda_2 = -1$					N+1	2
$-1 < \lambda_2 < 0$			2	1	2	1
$\lambda_2 = 0$						
$0 < \lambda_2 < 1$						
$\lambda_2 = 1$	2	N+1				
$\lambda_2 > 1$	1	2				

Table 2: Ground energy degeneracy for odd sites

	$\lambda_1 < -1$	$\lambda_1 = -1$	$-1 < \lambda_1 < 0$		$\lambda_1 = 0$	$0 < \lambda_1 \leq 1$		$\lambda_1 > 1$	
$\lambda_2 < -1$	2	2	$\lambda_2 \leq -\lambda_1$	$\lambda_2 > -\lambda_1$	2	$\lambda_2 \leq -\lambda_1$	$\lambda_2 > -\lambda_1$	2	4
$\lambda_2 = -1$									
$-1 < \lambda_2 < 0$			2	2	2	4	2	2	4
$\lambda_2 = 0$									
$0 < \lambda_2 < 1$									
$\lambda_2 = 1$					4				
$\lambda_2 > 1$									

In the table 1, for even numbers of sites,  $\lambda_1$  and  $\lambda_2$  must satisfy certain conditions to achieve degeneracy. Specifically, when  $\lambda_1 = -1$  and  $\lambda_2 = 1$ , or  $\lambda_1 = 1$  and  $\lambda_2 = -1$ , the observed degeneracy exceeds expectations. These cases represent accidental degeneracies that can be disregarded when perturbations are introduced into the system.

In the table 2, for odd numbers of sites, similar accidental degeneracies can occur. For example, when  $\lambda_1 = 0$  and  $\lambda_2 = 0$ , the degeneracy increases to  $2^N$ . In this situation, the Hamiltonian takes the following form:

$$\hat{H} = \sum_{i=1}^N S_{ix} S_{(i+1)x} \tag{18}$$

It is obvious that this hamiltonian has larger degeneracy. It has the relation with the symmetry of the system.

### 3.1.6. Symmetry of the ground state

Degeneracy is closely related to symmetries. Therefore, it is essential to understand the symmetries of the states.

- *S* (Spin Flip Operator): In the  $S = 1$  block, the basis states are spin flip symmetric. In the  $S = -1$  block, the basis states are spin flip anti-symmetric.
- *P* (Parity Operator): In the  $P = 1$  block, the basis states are inversion symmetric. In the  $P = -1$  block, the basis states are inversion anti-symmetric.
- *R* (Rotation Operator): In the  $R = 0$  block, there is no rotation. In the  $R = 1$  block, the chain is translated by one lattice site, and so on.

Table 3: Ground state symmetry for even sites

	$\lambda_1 < -1$	$\lambda_1 = -1$	$-1 < \lambda_1 < 1$		$\lambda_1 = 1$	$\lambda_1 > 1$
$\lambda_2 < -1$	$S=-1$	$S=-1$	$\lambda_1 = -\lambda_2$	$\lambda_1 \neq -\lambda_2$	$S=1, P=1, R=0$ or $S=-1, P=1, R=0$	$S=1, P=1, R=0$
$\lambda_2 = -1$	$P=1$	$P=1$	$S=-1$			$S=-1, P=-1, R=N/2$ or $S=1, P=1, R=0$
$-1 < \lambda_2 < 0$	$R=0$	$R=0$	$P=1$	$R=0$ or $S=-1$	$S=-1, P=-1, R=N/2$	$S=-1, P=-1, R=N/2$
$\lambda_2 = 0$			$R=0$ or $S=-1$			
$0 < \lambda_2 < 1$			$P=-1$			
$\lambda_2 = 1$	$S=-1, P=1, R=0$ or $S=1, P=1, R=0$		$P=-1$			
$\lambda_2 > 1$	$S=1, P=1, R=0$	$S=-1, P=-1, R=N/2$ or $S=1, P=1, R=0$	$R=N/2$			

Table 4: Ground state symmetry for odd sites

	$\lambda_1 \leq -1$	$\lambda_1 = 0$		$\lambda_1 = 0$	$0 < \lambda_1 \leq 1$		$\lambda_1 > 1$	
$\lambda_2 < -1$	$P=1$	$\lambda_2 \leq -\lambda_1$	$\lambda_2 > -\lambda_1$	$S=\pm 1, P=1, R=0$	$\lambda_2 \leq -\lambda_1$	$\lambda_2 > -\lambda_1$	$\lambda_2 < -1$	$\lambda_2 \geq -1$
$\lambda_2 = -1$								
$-1 < \lambda_2 < 0$	$R=0$	$P=1$	$P=\pm 1$		$P=1$			
$\lambda_2 = 0$	$S=\pm 1$	$S=\pm 1$	$S=\pm 1$		$S=\pm 1$	$S=\pm 1$	$P=1$	$S=\pm 1$
$0 < \lambda_2 < 1$				$R=0$			$P=\pm 1$	$P=\pm 1$
$\lambda_2 = 1$				$S=\pm 1$	$R=0$		$R=0$	
$\lambda_2 > 1$				$P=\pm 1$				

In the table 3 and 4, we have ignored the accidental symmetries. For even numbers of sites, we observe that the ground states occur only when  $R=0$  or  $R=N/2$ , corresponding to no rotation or a half rotation, respectively. Additionally, the degeneracy changes as  $\lambda_1$  and  $\lambda_2$  vary. For instance, when  $\lambda_1 < -1$  and  $\lambda_2 = 1$ , the degeneracy is 2. In this case, two ground states can be interpreted as a combination of the states when  $\lambda < 1$  and  $\lambda_1 > 1$ . This is analogous to the ground state shifting from  $|S = -1, P = 1, R = 0\rangle$  to  $|S = 1, P = 1, R = 0\rangle$  as  $\lambda_2$  changes from less than 1 to more than 1. During this transition, the degeneracy is broken. A similar phenomenon occurs when  $\lambda_1 > 1$ . For odd numbers of sites, the minimum ground state degeneracy is 2. When the ground state degeneracy is 4, it corresponds to the states  $|S = \pm 1, P = \pm 1\rangle$ . When the energy degeneracy is 2, the ground state must be of the form  $|S = \pm 1, P = 1, R = 0\rangle$ .

### 3.2. Numerical study of 1D Bose-Hubbard model

The earliest investigations into bosons' behavior in a lattice can be traced back to Philip Anderson's theory on localization phenomena in 1963[16]. The critical work for the Bose-Hubbard model is indeed the 1998 paper by Jaksch et al., which provided a theoretical framework for realizing the Bose-Hubbard model with cold atoms in optical lattices.[17] Immanuel Bloch and his colleagues at the University of Munich first experimentally realized the Bose-Hubbard model in optical lattices and observed the superfluid to Mott insulator transition. This achievement marked the experimental confirmation of the Bose-Hubbard model's predictions[18]. The absence of disorder and the low temperatures at which these experiments are conducted make such systems ideal for studying quantum phase transitions. Theoretically, the simplest Hamiltonian that describes a system of bosonic atoms in an optical lattice is the Bose-Hubbard model. This model can be expressed as follows:

$$\hat{H} = -t \sum_{\langle ij \rangle} b_i^\dagger b_j + \frac{U}{2} \sum_i n_i(n_i - 1) - \mu \sum_i n_i \quad (19)$$

#### • Mott Insulator

in the strong interaction regime, which means  $U \gg t$ , we can set  $t = 0$  and the 1D Hamiltonian reduces to

$$\hat{H} = \sum_{i=1}^N \hat{h}_i = \sum_{i=1}^N \frac{U}{2} \hat{n}_i(\hat{n}_i - 1) - \mu \hat{n}_i \quad (20)$$

Different states are now decoupled. The number states are the eigenstates for  $\hat{H}$ , which means in order to get the ground state, we need to find the smallest value of  $h_i$ . Then we obtain

$$n_i = \max\{0, \lfloor \frac{\mu}{U} \rfloor + 1\} \quad (21)$$

it means the number of particle per site is a specific integer number due to the ratio of  $U$  and  $\mu$ . If we add a particle into one site, which means there is a particle excitation, there will be some change in energy.

$$\Delta E_p = \left[ \frac{U}{2} (n_i + 1)n_i - \mu(n_i + 1) \right] - \left[ \frac{U}{2} n_i(n_i - 1) - \mu n_i \right] = U n_i - \mu > 0 \quad (22)$$

This implies that there will be energy gaps in the system. Adding a particle to the system requires significant changes. This phase is referred to as a Mott insulator. Unlike insulators in band theory, where the insulating property arises from the band structure, a Mott insulator's insulating behavior is due to strong interactions between particles.

In real world, the total particle in a system  $\sum_i^L n_i = Nb$  in the strong interaction ( $t=0$ ). The Hamiltonian becomes

$$\hat{H} = -\left(\frac{U}{2} + \mu\right)Nb + \frac{U}{2} \sum_i^L n_i^2 \quad (23)$$

where  $L$  is the number of sites and  $Nb$  is the total number of particles. We are primarily concerned with the ground state, which corresponds to minimizing the Hamiltonian. Therefore, our goal is to minimize  $\sum_i^L n_i^2$ . By applying the Cauchy-Schwarz inequality, we have:  $\sum_i^L 1^2 \sum_i^L n_i^2 \geq (\sum_i^L n_i)^2$ . Thus,  $\sum_i^L n_i^2 \geq \frac{Nb^2}{L}$ . Equality holds when  $n_i = \frac{Nb}{L}$ . Since  $n_i$  must be a non-negative integer, we need to distinguish between the cases  $U > 0$  and  $U < 0$

(i)  $U > 0$

(a)  $Nb \leq L$

For the ground state,  $n_i$  could only be 1 or 0. For  $Nb$  sites, there are 1 particle in each site. For the else sites ( $L - Nb$ ), there is 0 particle. Then the ground energy becomes:

$$E = \left(\frac{U}{2} + \mu\right)Nb + \frac{U}{2}Nb = -\mu Nb \quad (24)$$

The energy is proportion to the chemical potential.

(b)  $Nb > L$

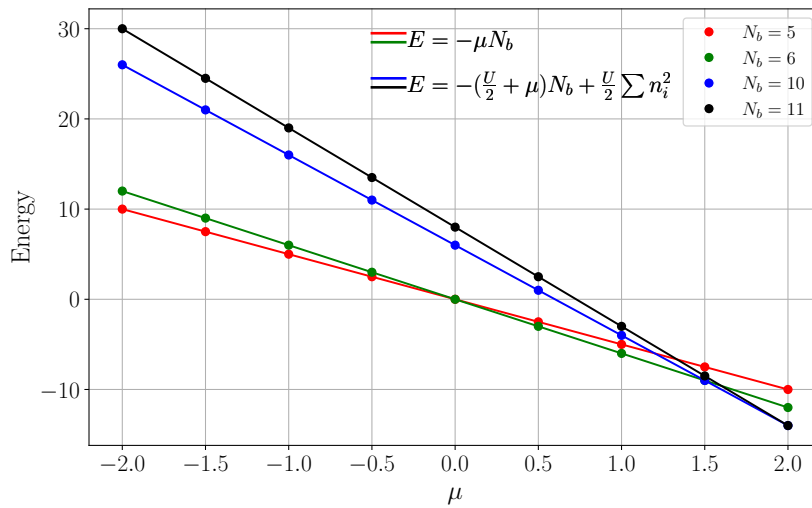
The average should be  $n_i = [\frac{Nb}{L} + \frac{1}{2}]$ . However, sometimes  $n_i * L \neq Nb$ . Therefore, due to the total particle conservation, particle on each site may not perfectly equals to  $n_i$ .

(ii)  $U < 0$

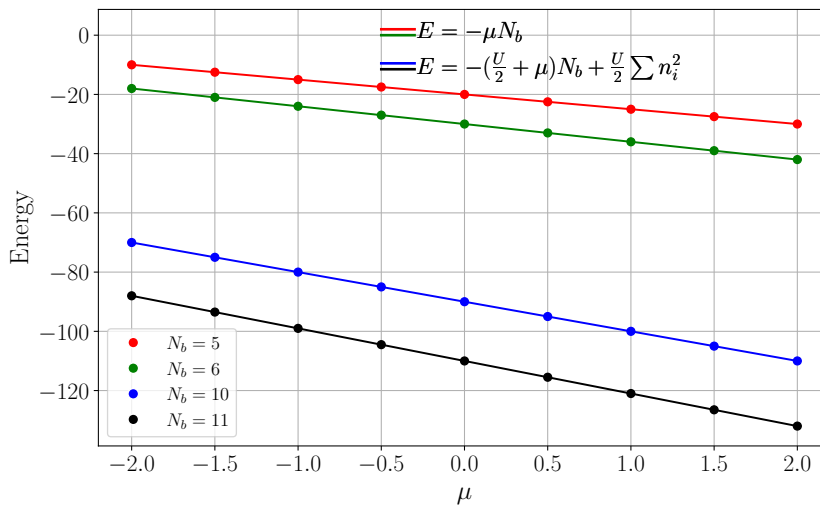
If we want to maximize  $\sum_i^L n_i^2$ , we need to place  $Nb$  particles at one site and no particle at other sites. Then eq(23) becomes:

$$E = -(\frac{U}{2} + \mu)Nb + \frac{U}{2}Nb^2 \tag{25}$$

We want to plot the energy with different particles. The maximum ground energy occurs when  $Nb = \max([\frac{1}{2} + \frac{\mu}{U}], 0)$ . In the figure 9 we choose  $U = -2$  and when  $\mu \geq 1$ , the maximum energy occurs at  $Nb=0$ . When  $\mu < 1$ , the maximum energy occurs at  $Nb = [\frac{1}{2} + \frac{\mu}{U}]$ .



(a) repulsive interaction(U=2)



(b) attractive interaction(U=-2)

Figure 9: Energy for different chemical potential. The dots are numerical results[15] and lines are theoretical results.

• Superfluid

In the weak interaction regime, which means  $t \gg U$ , the onsite interaction is negligible and the Hamiltonian becomes

$$\hat{H} = -t \sum_{\langle ij \rangle} b_i^\dagger b_j - \mu \sum_i n_i \quad (26)$$

we can use Fourier transition  $\hat{b}_k = \frac{1}{\sqrt{L}} \sum_{j=1}^L \hat{b}_j e^{-ikj}$ , then the Hamiltonian becomes

$$\hat{H} = \sum_k (\epsilon_k - \mu) \hat{b}_k^\dagger \hat{b}_k, \quad \epsilon_k = -2t \cos k \quad (27)$$

Therefore, the ground state for this Hamiltonian is when all particles condense into the  $k = 0$  state in the Fourier space

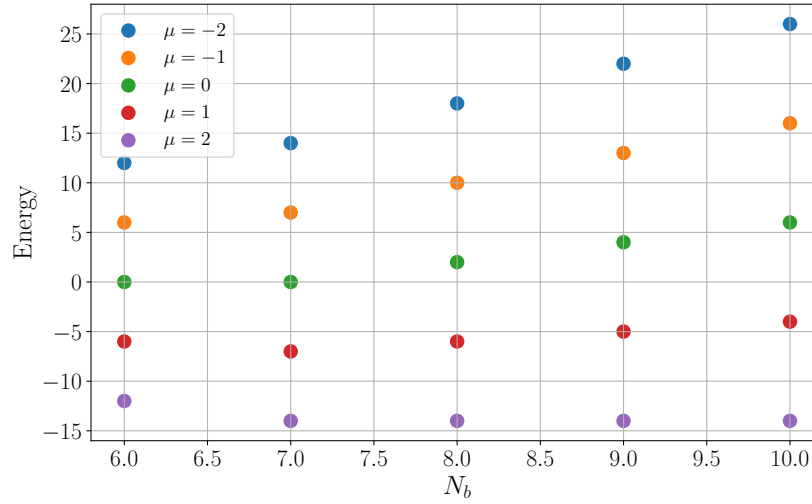
$$|\Psi_{SF}\rangle = \frac{1}{m!} (\hat{b}_{k=0}^\dagger)^m |0\rangle \quad (28)$$

$$\hat{b}_{k=0} = \sum_{i=1}^L \hat{b}_i$$

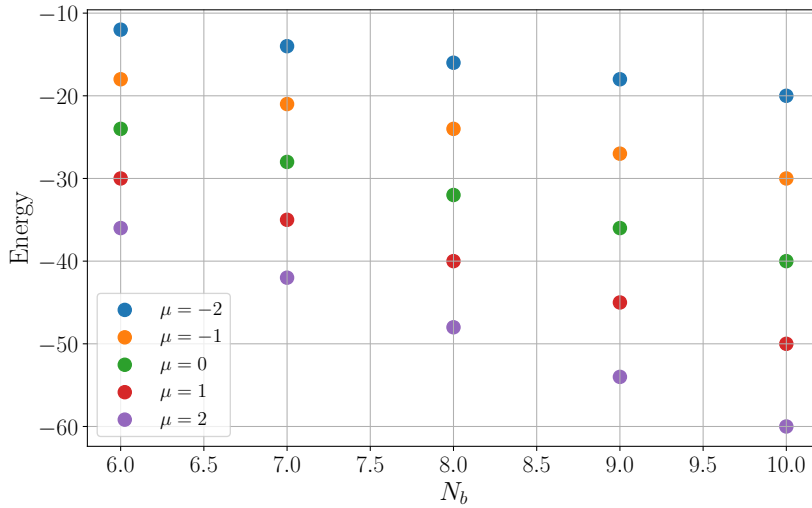
Then the ground energy becomes:

$$\hat{H}_{ground} = (-2t - \mu) \hat{b}_{k=0}^\dagger \hat{b}_{k=0} = (-2t - \mu) \sum_{j=1}^L \hat{b}_j^\dagger \hat{b}_j = (-2t - \mu) \sum_{j=1}^L n_j = (-2t - \mu) Nb \quad (29)$$

Due to the delocalization of particles, this state characterizes the superfluid phase. According to Landau's theory, a superfluid phase occurs if  $V_c = \min(\frac{\epsilon|q|}{|q|}) \neq 0$ , where  $\epsilon|q|$  represents the energy dispersion relation.



(a) Mott Insulator



(b) Superfluid

Figure 10: Energy for different particles in different phase[15]

We start with the Hamiltonian of the Bose-Hubbard model and use exact diagonalization to solve it. In the following discussion, we apply periodic boundary conditions, meaning that the beginning and end of the chain are connected. We utilize the constrained Bose-Hubbard model, where the number of particles and sites are fixed, just like in the figure 10. In a real-world scenario, both the number of particles and the number of sites would approach infinity. However, due to computational limitations, we are constrained to calculations with a finite number of particles and sites.

### 3.2.1. Exact diagonalization

It is evident that we use the canonical ensemble to calculate the Hamiltonian. Consequently, we set the chemical potential  $\mu$  to zero. By definition, the chemical potential represents the energy required to add or remove a particle from the system. There are various methods to calculate the chemical potential and assess whether the system is in the Mott phase or the superfluid phase. We can use definition  $\mu^+(L) = E_0(L, N_b + 1)$ ,  $\mu^-(L) = E_0(L, N) - E_0(L, N - 1)$  and calculate  $\Delta(L) = \mu^+(L) - \mu^-(L)$ [19], where  $E_0$  is the ground state of this system. The gap  $\Delta$  is finite for the Mott insulator. We can also use the basic definition to estimate Mott insulator or Superfluid phase[20]. In this paper,  $\mu(N_b) = E_0(N_b + 1) - E_0(N_b)$  and compressibility  $\kappa = \frac{\partial \rho}{\partial \mu} = \frac{1}{\mu(N_b+1) - \mu(N_b)}$ , where  $\rho$  is  $\frac{N_b}{L}$ . Moreover, in the ground state, the particle density on each site is uniform and equals  $\rho$ . The compressibility is a key distinguishing feature between a Mott insulator and a superfluid. Mott

insulators exhibit zero compressibility, reflecting their fixed particle number and the insulating behavior induced by strong interactions. In contrast, superfluids have finite compressibility, which indicates their ability to adjust particle density and flow without resistance. Therefore, in exact diagonalization, the difference in compressibility can be used to determine whether the system is in a Mott insulator phase or a superfluid phase.

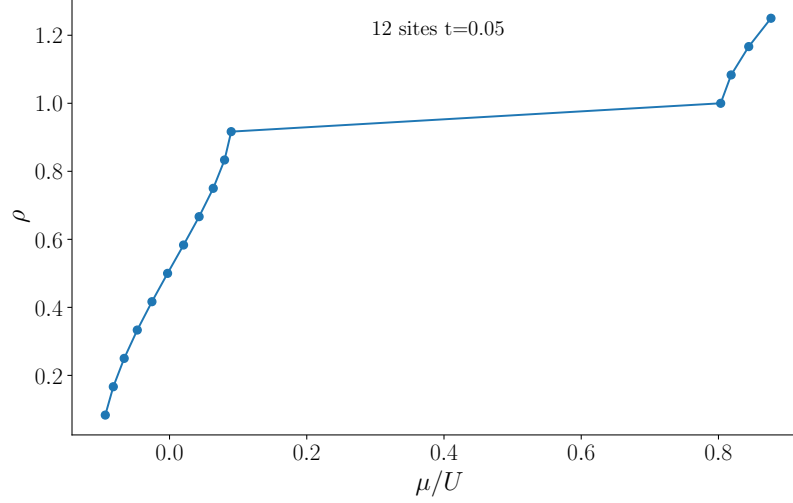


Figure 11: The number density  $\rho$  as a function of chemical potential  $\mu$  when we set  $t/U = 0.05$

The slope of the figure 11 is compressibility  $\kappa$ . Clearly, a phase transition occurs when  $\mu \approx 0.1$ . Based on the previous discussion, when the slope of the compressibility is zero, the system is in the Mott insulator phase. Conversely, when the slope is finite, the system is in the superfluid phase. (Due to the limitations of lattice size, the slope may not be perfectly smooth.) By varying the hopping parameter  $t$ , we can observe different phase transition points, which can then be plotted on a phase diagram, just like in the figure 12.

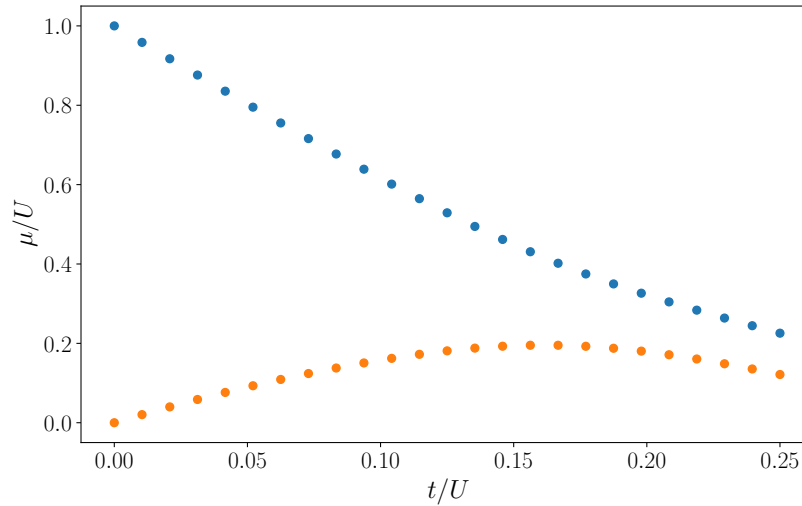


Figure 12: The phase transition when  $U=1$ . The part enclosed by two lines is Mott insulator phase and the outside part is superfluid phase

### 3.2.2. Mean-field theory

We use the mean field theory to approximate the hamiltonian.

$$\hat{b}_i^\dagger \hat{b}_m = (\langle \hat{b}_i^\dagger \rangle + \hat{b}_i^\dagger - \langle \hat{b}_i^\dagger \rangle)(\langle \hat{b}_j \rangle + \hat{b}_j - \langle \hat{b}_j \rangle) \approx \langle \hat{b}_i^\dagger \rangle \hat{b}_j + \hat{b}_i^\dagger \langle \hat{b}_j \rangle - \langle \hat{b}_i^\dagger \rangle \langle \hat{b}_j \rangle \quad (30)$$

Therefore, the hopping hamiltonian becomes:

$$\hat{H}_t = -t \sum_{\langle ij \rangle} \langle \hat{b}_i^\dagger \rangle \hat{b}_j + \hat{b}_i^\dagger \langle \hat{b}_j \rangle - \langle \hat{b}_i^\dagger \rangle \langle \hat{b}_j \rangle = 2tb_0^2 N_s - 2tb_0 \sum_j \hat{b}_j^\dagger + \hat{b}_j \quad (31)$$

In this equation, we suppose the transition invariant in the system and due to the phase we choose. Then the order parameter must be real constant so that we choose  $\langle \hat{b}_i^\dagger \rangle = \langle \hat{b}_j \rangle = b_0$ .  $N_s$  means total number of sites. The total Hamiltonian can be expressed as:

$$H = 2tb_0^2 N_s + \sum_j -2tb_0(\hat{b}_j^\dagger + \hat{b}_j) - \mu \hat{b}_j^\dagger \hat{b}_j + \frac{U}{2} \hat{b}_j^\dagger \hat{b}_j (\hat{b}_j^\dagger \hat{b}_j - 1) \quad (32)$$

The summation term is the mean field term, which includes the hopping term and onsite energy term. In order to calculate this Hamiltonian, we need to in the  $|n_b\rangle$  basis, like  $|n_b\rangle = 0, |n_b\rangle = 1, |n_b\rangle = 2 \dots$ . Due to the no upper limit of  $n_b$ , we need to do

truncation  $n_{b,max} = n$ . Then in this basis, the matrix of  $\hat{b}_j = \begin{pmatrix} 0 & 1 & 0 & 0 & \dots & 0 \\ 0 & 0 & \sqrt{2} & 0 & \dots & 0 \\ 0 & 0 & 0 & \sqrt{3} & \dots & 0 \\ \vdots & \vdots & \vdots & \ddots & \ddots & \vdots \\ 0 & 0 & 0 & 0 & \dots & \sqrt{n} \\ 0 & 0 & 0 & 0 & \dots & 0 \end{pmatrix}$ . We now have an  $(n+1) \times (n+1)$

matrix. As  $n$  increases, the results become more accurate. To build the Hamiltonian for each site, we need to include the order parameter  $b_0$ . The procedure is as follows:

- 1. Initial Guess: Start with an initial guess for  $b_0$  and incorporate it into the Hamiltonian.
- 2. Diagonalization: Diagonalize the Hamiltonian to obtain the ground state and calculate the average value of  $b_j$ .
- 3. Use the average value of  $b_j$  as the new  $b_0$  and substitute it back into the Hamiltonian.
- 4. Repeat this process several times until the difference between the new  $b_0$  and the old  $b_0$  is within an acceptable range.

The average particle density per site can then be used to determine whether the system is in the Mott insulator phase or the superfluid phase. Then we can plot the phase diagram as figure 13.

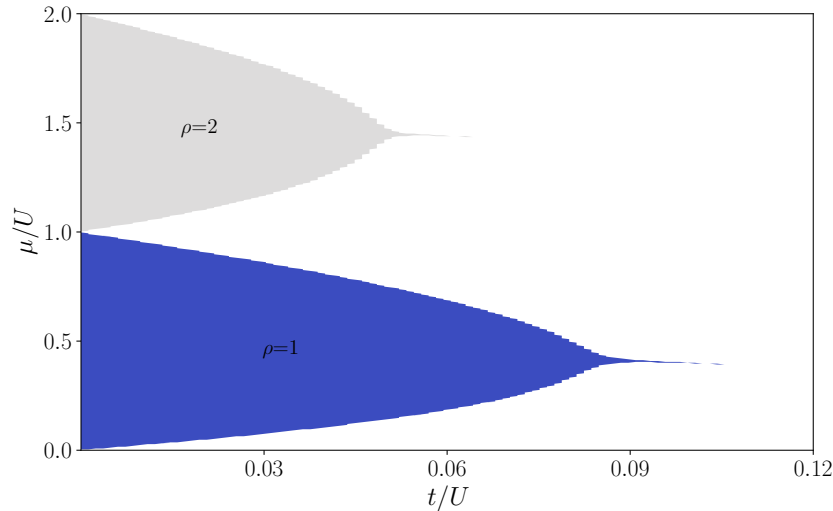


Figure 13: Mean field phase diagram

Moreover, we can also treat the hopping term as a perturbation, while the interaction energy term remains the non-perturbative part. Using second-order perturbation theory, the ground state energy can be expressed as:

$$E'(n_b) = E(n_b) + \langle n_b | \hat{H}_{site}^t | n_b \rangle + \sum_{m \neq n_b} \frac{|\langle m | \hat{H}_{site}^t | n_b \rangle|^2}{E_b(n_b) - E_b(m)} + \dots \quad (33)$$

The first-order perturbation term  $\langle n_b | \hat{H}_{\text{site}}^t | n_b \rangle$  is zero because the annihilation and creation operators in the hopping Hamiltonian do not contribute when acting on the state  $|n_b\rangle$ . Additionally, all odd-order perturbation terms are zero. Therefore, the Hamiltonian can be expressed as:

$$E'(n_b) = E(n_b) + A(n_b)b_0^2 + B(n_b)b_0^4 \quad (34)$$

It is the same as Landau free energy. Due to the Landau theory, in the  $B(n_b) > 0$  situation, the transition occurs at  $A(n_b) = 0$ . Then we get:

$$\frac{t}{U} = \frac{(n_b - \frac{\mu}{U})(\frac{\mu}{U} + 1 - n_b)}{2(\frac{\mu}{U} + 1)} \quad (35)$$

We can compare the theoretical phase diagram with numerical phase diagram in the figure 14.

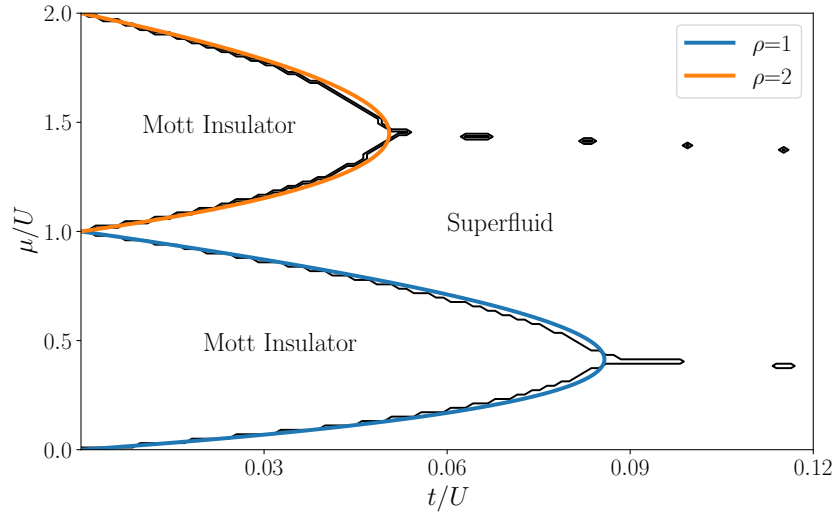


Figure 14: The smooth curve is the theoretical line and the zigzag line is the mean field exact diagonalization.

However, in 1D systems, quantum fluctuations are more pronounced compared to higher dimensions. Mean-field theory approximates the behavior of particles by averaging their interactions with surrounding particles. While this approach can be effective in higher dimensions, where fluctuations are relatively small, it fails in 1D systems where fluctuations play a critical role. Therefore, using mean-field theory to calculate the 1D Bose-Hubbard model is not appropriate.

### 3.2.3. Gutzwiller variational ansatz

To describe transitions between the superfluid and insulating states we use Gutzwiller variational wavefunction[21].

$$|\Psi_G\rangle = \prod_i (f_0 + f_1 b_i^\dagger + f_2 \frac{b_i^{\dagger 2}}{\sqrt{2}} + \dots + f_n \frac{b_i^{\dagger n}}{\sqrt{n!}}) |0\rangle \quad (36)$$

Here the coefficient is normalized. After minimizing the wavefunction with respect to the normalization constraint, we obtain the following equation:

$$H_U + H_\mu = \sum_n (-n\mu + \frac{U}{2}n(n-1)) |f_n|^2 \quad (37)$$

$$H_t = -2t|f_0^* f_1 + \sqrt{2}f_1^* f_2 + \sqrt{3}f_2^* f_3 + \dots|^2 \quad (38)$$

$$H_{Gutzwiller} = H_U + H_\mu + H_t \quad (39)$$

To numerically calculate the phase transition of the Gutzwiller Hamiltonian, we use the simulated annealing (SA) algorithm. By employing normalized random functions to simulate the Gutzwiller wavefunction, we can construct the Gutzwiller Hamiltonian. We then generate another Gutzwiller Hamiltonian using a different normalized random function. The decision to accept the new wavefunction is based on the Metropolis criterion, which involves setting an acceptance rate. By calculating the average particle density per site, we can determine the phase of the system. This approach allows us to construct the phase diagram as shown in the figure 15.

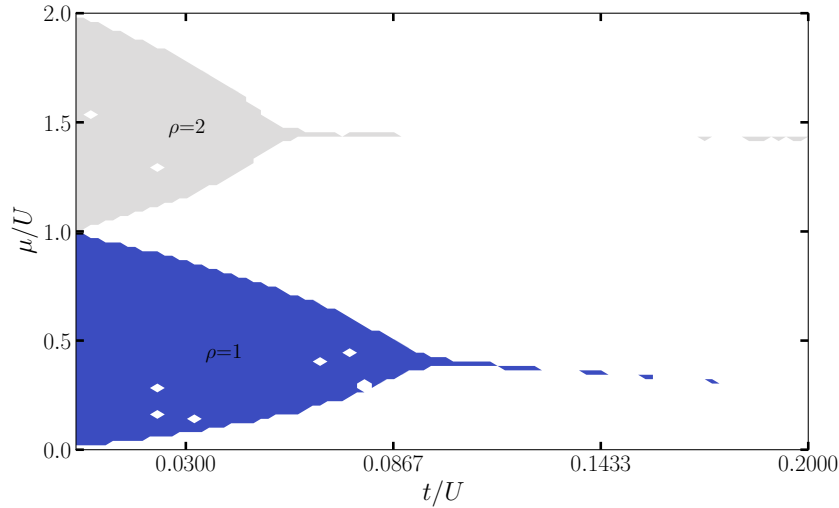


Figure 15: Gutzwiller phase diagram

We can compare phase diagram in the figure 16.

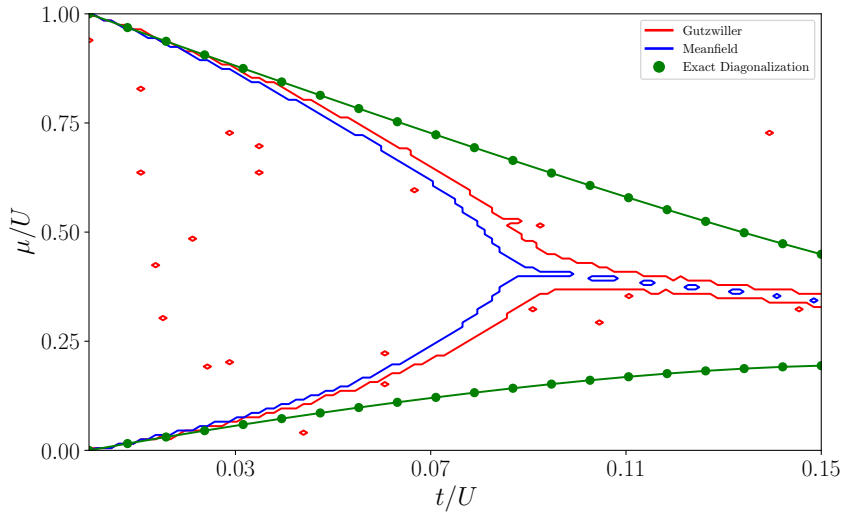


Figure 16: Red plot is Gutzwiller, blue plot is meanfield and green plot is Exact Diagonalization. The area enclosed by a curve is Mott Insulator and outside is Superfluid phase.

### 3.2.4. Correlation function

Moreover, we can use correlation function  $\langle b_0^\dagger b_i \rangle$  to verify the phase transition. In the superfluid phase, the system exhibits long range coherence so that the attenuation behavior of  $b_0^\dagger b_i$  is usually polynomial.

$$\langle b_0^\dagger b_i \rangle \sim \frac{1}{r^\alpha} \tag{40}$$

where  $r = |i - 0|$ ,  $\alpha$  is a positive constant. The long range polynomial attenuation reflects the existence of long range quantum coherence and coherent fluctuations in the superfluid phase. In the Mott insulator phase, the motion of particles in the system is inhibited and the long-range quantum coherence disappears. Therefore,  $b_0^\dagger b_i$  decays exponentially.

$$\langle b_0^\dagger b_i \rangle \sim e^{-\frac{r}{\xi}} \tag{41}$$

where  $\xi$  is the associated length of the system and is usually finite. Due to the symmetry of bose hubbard model, we only consider half of the chain. From the figure 17, we know that when  $t$  is very small (Mott insulator phase), correlation function decays exponentially.

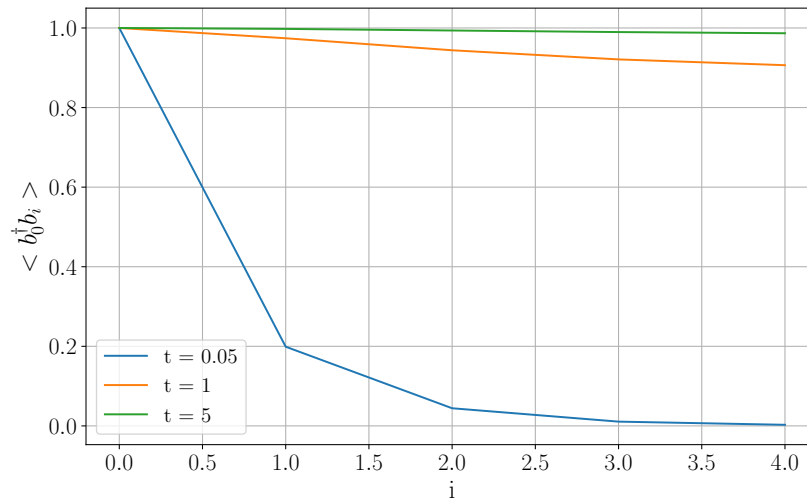


Figure 17: Correlation function  $\langle b_0^\dagger b_i \rangle$  for different particle sites when we set different  $t$ [15]

When the number of sites  $t$  is large (indicating the superfluid phase), the correlation function decays polynomially. To determine the phase transition, we can use exponential fitting. If the fit residual is sufficiently small, we can conclude that the system is in the Mott insulator phase. Conversely, if the residual is large, the system is in the superfluid phase. To calculate the transition point from the Mott insulator phase to the superfluid phase, we require statistical analysis. First, we fit the correlation function with an exponential function. Then, we calculate the root-mean-square error (RMSE) of the fit, as illustrated in Fig. 17.

$$RMSE = \sqrt{\frac{1}{n} \sum_{i=1}^n (\langle b_0^\dagger b_i \rangle - (ae^{bi} + c))^2} \tag{42}$$

where  $a, b$  and  $c$  are fit parameters of the correlation function.

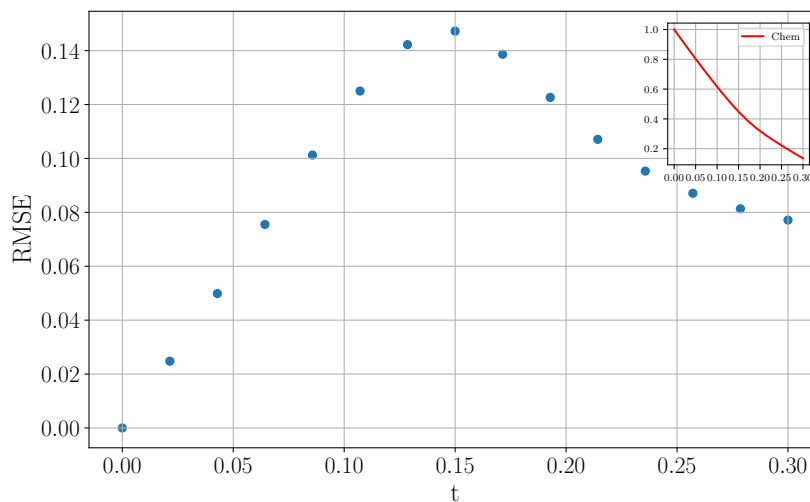


Figure 18: The root-mean-square error for different  $t$ . The subplot on the upper right is chemical potential in this system.[15]

In the figure 18, at about  $t=0.12$ , residual becomes the biggest, which means this system turns from mott insulator into superfluid. The result is similar to the mean field theory results. It is a great verification of our phase transition.

#### 4. Conclusion

In this paper, we have summarized a variety of tools, including the RWA approximation, symmetry operators, and effective Hamiltonians, which are highly useful in the study of strongly correlated systems for simplifying complex Hamiltonians. We aimed to capture the essential technical aspects of these approaches and provide examples of their application in various physical contexts. We gained deep insights into the 1D spin model by employing three symmetry operators—parity operator, spin flip operator, and rotation operator—to simplify the Hamiltonian. This allowed us to determine ground state properties such as degeneracies and symmetries.

Additionally, we studied the 1D Bose-Hubbard model using three methods—exact diagonalization, mean-field theory, and Gutzwiller wave approximation. We constructed phase diagrams from these methods and used correlation functions to verify the results.

#### References

- [1] T. Ozawa, H. M. Price, A. Amo, N. Goldman, M. Hafezi, L. Lu, M. C. Rechtsman, D. Schuster, J. Simon, O. Zilberberg *et al.*, “Topological photonics,” *Reviews of Modern Physics*, vol. 91, no. 1, p. 015006, 2019.
- [2] A. Y. Kitaev, “Fault-tolerant quantum computation by anyons,” *Annals of physics*, vol. 303, no. 1, pp. 2–30, 2003.
- [3] M. Z. Hasan and C. L. Kane, “Colloquium: topological insulators,” *Reviews of modern physics*, vol. 82, no. 4, pp. 3045–3067, 2010.
- [4] G. Jackeli and G. Khaliullin, “Mott insulators in the strong spin-orbit coupling limit: from heisenberg to a quantum compass and kitaev models,” *Physical review letters*, vol. 102, no. 1, p. 017205, 2009.
- [5] S. G. Stewart, “Heavy-fermion systems,” *Reviews of Modern Physics*, vol. 56, no. 4, p. 755, 1984.
- [6] S. Bravyi, D. P. DiVincenzo, and D. Loss, “Schrieffer–wolf transformation for quantum many-body systems,” *Annals of physics*, vol. 326, no. 10, pp. 2793–2826, 2011.
- [7] M. Wagner, “Unitary transformations in solid state physics,” 1986.
- [8] A. H. MacDonald, S. M. Girvin, and D. t. Yoshioka, “t u expansion for the hubbard model,” *Physical Review B*, vol. 37, no. 16, p. 9753, 1988.
- [9] P. Phillips, Y. Wan, I. Martin, S. Knysh, and D. Dalidovich, “Superconductivity in a two-dimensional electron gas,” *Nature*, vol. 395, no. 6699, pp. 253–257, 1998.
- [10] A. Kale, J. H. Huhn, M. Xu, L. H. Kendrick, M. Lebrat, C. Chiu, G. Ji, F. Grusdt, A. Bohrdt, and M. Greiner, “Schrieffer-wolff transformations for experiments: Dynamically suppressing virtual doublon-hole excitations in a fermi-hubbard simulator,” *Physical Review A*, vol. 106, no. 1, p. 012428, 2022.
- [11] R. Oliveira and B. M. Terhal, “The complexity of quantum spin systems on a two-dimensional square lattice,” *arXiv preprint quant-ph/0504050*, 2005.
- [12] J. Kempe, A. Kitaev, and O. Regev, “The complexity of the local hamiltonian problem,” *Siam journal on computing*, vol. 35, no. 5, pp. 1070–1097, 2006.
- [13] E. Brion, L. H. Pedersen, and K. Mølmer, “Adiabatic elimination in a lambda system,” *Journal of Physics A: Mathematical and Theoretical*, vol. 40, no. 5, p. 1033, 2007.
- [14] L. Onsager *et al.*, “A two-dimensional model with an order-disorder transition,” *Phys. Rev.*, vol. 65, no. 3, pp. 117–149, 1944.
- [15] P. Weinberg and M. Bukov, “QuSpin: a Python package for dynamics and exact diagonalisation of quantum many body systems. Part II: bosons, fermions and higher spins,” *SciPost Phys.*, vol. 7, p. 020, 2019. [Online]. Available: <https://scipost.org/10.21468/SciPostPhys.7.2.020>
- [16] A. Aspect and M. Inguscio, “Anderson localization of ultracold atoms,” *Physics today*, vol. 62, no. 8, pp. 30–35, 2009.
- [17] D. Jaksch, C. Bruder, J. I. Cirac, C. W. Gardiner, and P. Zoller, “Cold bosonic atoms in optical lattices,” *Physical Review Letters*, vol. 81, no. 15, p. 3108, 1998.
- [18] M. Greiner, O. Mandel, T. Esslinger, T. W. Hänsch, and I. Bloch, “Quantum phase transition from a superfluid to a mott insulator in a gas of ultracold atoms,” *nature*, vol. 415, no. 6867, pp. 39–44, 2002.
- [19] S. Ejima, H. Fehske, and F. Gebhard, “Dynamic properties of the one-dimensional bose-hubbard model,” *Europhysics Letters*, vol. 93, no. 3, p. 30002, 2011.

- [20] G. G. Batrouni and R. T. Scalettar, “World-line quantum monte carlo algorithm for a one-dimensional bose model,” *Physical Review B*, vol. 46, no. 14, p. 9051, 1992.
- [21] E. Demler and T. Kitagawa, “Strongly correlated systems in atomic and condensed matter physics,” *Lecture notes for Physics*, vol. 284, p. 28, 2011.
- [22] J. J. Sakurai and J. Napolitano, *Modern quantum mechanics*. Cambridge University Press, 2020.

## Appendix

### Appendix A: Detailed derivation of lambda system

#### The dipole-electric field interaction term in the interaction picture

The interaction term can be expressed as:

$$V = -\vec{d} \cdot \vec{E} = -\vec{d}^{\dagger} \cdot \vec{E}^{\dagger} - \vec{d}^{\dagger} \cdot \vec{E}^{-} - \vec{d}^{\dagger} \cdot \vec{E}^{-} - \vec{d}^{\dagger} \cdot \vec{E}^{\dagger} \quad (43)$$

Remembering that  $E_a$  only acts on  $|a\rangle$  and  $E_b$  only acts on  $|b\rangle$ , we define  $\Omega_i = -\frac{\langle e|\vec{d}\cdot\vec{E}_i|i\rangle}{\hbar}$ ,  $i = a, b$ .

$$\begin{aligned} V &= \left(\frac{\Omega_a^*}{2} e^{-i\omega_a^{(L)}t} \sigma_1 + \frac{\Omega_b^*}{2} e^{-i\omega_b^{(L)}t} \sigma_2\right) + \left(\frac{\Omega_a}{2} e^{i\omega_a^{(L)}t} \sigma_1^{\dagger} + \frac{\Omega_b}{2} e^{i\omega_b^{(L)}t} \sigma_2^{\dagger}\right) \\ &+ \left(\frac{\Omega_a^*}{2} e^{i\omega_a^{(L)}t} \sigma_1 + \frac{\Omega_b^*}{2} e^{i\omega_b^{(L)}t} \sigma_2\right) + \left(\frac{\Omega_a}{2} e^{-i\omega_a^{(L)}t} \sigma_1^{\dagger} + \frac{\Omega_b}{2} e^{-i\omega_b^{(L)}t} \sigma_2^{\dagger}\right) \\ &= V_{++} + V_{--} + V_{+-} + V_{-+} \end{aligned} \quad (44)$$

We put V in the interaction picture.

$$V_I = e^{\frac{i}{\hbar}H_0t} V e^{-\frac{i}{\hbar}H_0t} = e^{\frac{i}{\hbar}H_0t} (V_{++} + V_{--} + V_{+-} + V_{-+}) e^{-\frac{i}{\hbar}H_0t} \quad (45)$$

Take  $e^{\frac{i}{\hbar}H_0t} V_{++} e^{-\frac{i}{\hbar}H_0t} = \frac{\hbar\Omega_a^* e^{-i\omega_a^{(L)}t}}{2} e^{\frac{i}{\hbar}H_0t} \sigma_1 e^{-\frac{i}{\hbar}H_0t} + \frac{\hbar\Omega_b^* e^{-i\omega_b^{(L)}t}}{2} e^{\frac{i}{\hbar}H_0t} \sigma_2 e^{-\frac{i}{\hbar}H_0t}$  as an example. Here we give a very useful equation.

$$e^X A e^{-X} = A + [X, A] + \frac{1}{2!} [X, [X, A]] + \dots \quad (46)$$

Here  $X = \frac{i}{\hbar}H_0t$ ,  $A = \sigma_1 = |a\rangle\langle e|$ ,  $[X, A] = \frac{it}{\hbar}\hbar(\Delta - \omega_a)[|a\rangle\langle a|, |a\rangle\langle e|] + \frac{it}{\hbar}\hbar(\Delta - \omega_b)[|b\rangle\langle b|, |a\rangle\langle e|] + \frac{it}{\hbar}\hbar\Delta[|e\rangle\langle e|, |a\rangle\langle e|] = -it\omega_a |a\rangle\langle e|$ , so that

$$e^{\frac{i}{\hbar}H_0t} \sigma_1 e^{-\frac{i}{\hbar}H_0t} = \sigma_1 + (-it\omega_a)\sigma_1 + \frac{1}{2!}(-it\omega_a)^2\sigma_1 + \dots = e^{-it\omega_a}\sigma_1 \quad (47)$$

In the same way, we can derive that  $e^{\frac{i}{\hbar}H_0t} \sigma_2 e^{-\frac{i}{\hbar}H_0t} = e^{-it\omega_b}\sigma_2$ . Therefore  $e^{\frac{i}{\hbar}H_0t} V_{++} e^{-\frac{i}{\hbar}H_0t} = \frac{\hbar\Omega_a^*}{2} e^{-it(\omega_a + \omega_a^{(L)})} \sigma_1 + \frac{\hbar\Omega_b^*}{2} e^{-it(\omega_b + \omega_b^{(L)})} \sigma_2$ . In the same way, we can derive  $V_I$  as follows:

$$\begin{aligned} V_I &= \left(\frac{\hbar\Omega_a^*}{2} e^{-it(\omega_a + \omega_a^{(L)})} \sigma_1 + \frac{\hbar\Omega_b^*}{2} e^{-it(\omega_b + \omega_b^{(L)})} \sigma_2\right) \\ &+ \left(\frac{\hbar\Omega_a}{2} e^{it(\omega_a + \omega_a^{(L)})} \sigma_1^{\dagger} + \frac{\hbar\Omega_b}{2} e^{it(\omega_b + \omega_b^{(L)})} \sigma_2^{\dagger}\right) \\ &+ \left(\frac{\hbar\Omega_a^*}{2} e^{it(\omega_a - \omega_a^{(L)})} \sigma_1^{\dagger} + \frac{\hbar\Omega_b^*}{2} e^{it(\omega_b - \omega_b^{(L)})} \sigma_2^{\dagger}\right) \\ &+ \left(\frac{\hbar\Omega_a}{2} e^{-it(\omega_a - \omega_a^{(L)})} \sigma_1 + \frac{\hbar\Omega_b}{2} e^{-it(\omega_b - \omega_b^{(L)})} \sigma_2\right) \end{aligned} \quad (48)$$

#### unitary transformation

If we have a unitary transformation U and  $|\psi\rangle$  is the solution to the original Schrodinger equation. New state becomes  $|\tilde{\psi}\rangle = U|\psi\rangle$  and new Schrodinger equation becomes  $\tilde{H}|\tilde{\psi}\rangle = i\hbar\frac{\partial}{\partial t}|\tilde{\psi}\rangle$ . It is easy to prove that the relation between old Hamiltonian and new Hamiltonian:

$$\tilde{H} = U H U^{\dagger} + i\hbar\frac{\partial U}{\partial t} U^{\dagger} \quad (49)$$

In the lambda system example, we choose proper  $U$  as below and then apply it to the old  $\hat{H}$  in order to get a new  $\hat{H}$  like equation(10).

$$U = \begin{pmatrix} e^{-i\omega_a^{(L)}t} & 0 & 0 \\ 0 & e^{-i\omega_b^{(L)}t} & 0 \\ 0 & 0 & 1 \end{pmatrix} \quad (50)$$

## Rotating Wave Approximation

According to time-dependent perturbation theory, we have below:

$$i\hbar \frac{\partial}{\partial t} \hat{u}_I(t, t_0) = \hat{V}_I(t) \hat{u}_I(t, t_0) \quad (51)$$

where  $u_I(t, t_0)$  is the time-revolution operator in the interaction frame;  $V_I(t)$  is the perturbation if the total Hamiltonian  $H = H_0 + V(t)$  and  $V(t)$  is small. For  $u_I(t, t_0)$  we have following equation:

$$\hat{u}_I(t, t_0) = \sum_{n=0}^{\infty} \left(\frac{1}{i\hbar}\right)^n \int_{t_0}^t dt_1 \int_{t_0}^{t_1} dt_2 \dots \int_{t_0}^{t_{n-1}} dt_n \hat{V}_I(t_1) \hat{V}_I(t_2) \dots \hat{V}_I(t_n) \quad (52)$$

The transition amplitude from state m to state n is written as follows:

$$P_{n \leftarrow m}(t) = |\langle \psi_n^0 | \hat{u}(t, t_0) | \psi_m^0 \rangle|^2 = |\langle \psi_n^0 | \hat{u}_I(t, t_0) | \psi_m^0 \rangle|^2 \quad (53)$$

where  $|\psi_n^0\rangle$  and  $|\psi_m^0\rangle$  are unperturbed states which means the eigenstate of  $H_0$ . In our question, we need to know the amplitude from  $|a\rangle$  to  $|b\rangle$ . We expand the equation (52) into second order.

$$\hat{u}_I(t, t_0) = I - \frac{i}{\hbar} \int_{t_0}^t dt' V_I(t') + \left(\frac{-i}{\hbar}\right)^2 \int_{t_0}^t dt' \int_{t_0}^{t'} dt'' V_I(t') V_I(t'') \quad (54)$$

Because we need to calculate the amplitude from a to b, the interaction term must include terms similar to  $|b\rangle \langle a|$ . Otherwise, due to the orthogonal between  $|a\rangle$ ,  $|b\rangle$  and  $|e\rangle$ , other terms should be 0. Therefore, the first order perturbation becomes 0 because it doesn't include  $|b\rangle \langle a|$  term. After selecting the term includes  $|b\rangle \langle a|$ , the amplitude becomes:

$$P_{b \leftarrow a}(t) = \left| \left(\frac{-i}{\hbar}\right)^2 \int_{t_0}^t dt' \left( \frac{\hbar\Omega_b^*}{2} e^{-it'(\omega_b + \omega_b^{(L)})} + \frac{\hbar\Omega_b}{2} e^{-it'(\omega_b - \omega_b^{(L)})} \right) \int_{t_0}^{t'} dt'' \left( \frac{\hbar\Omega_a}{2} e^{it''(\omega_a + \omega_a^{(L)})} + \frac{\hbar\Omega_a^*}{2} e^{it''(\omega_a - \omega_a^{(L)})} \right) \right|^2 \quad (55)$$

after integrating, the transition probability including  $\omega_a + \omega_a^{(L)}$  is much smaller than that including  $|\omega_a - \omega_a^{(L)}|$ . The term including  $\omega_a + \omega_a^{(L)}$  can be neglected. This is called Rotating Wave Approximation: the fast rotating term like  $e^{it''(\omega_a + \omega_a^{(L)})}$  can be neglect.

## Appendix B: Scalar operator, vector operator and tensor operator

Electric field operator and dipole operator are vector operators.

### scalar operator

The generator of rotating is angular momentum. If the expectation value of an operator is invariant under rotation, we call this operator the scalar operator. We have a state  $|\psi\rangle$  and after rotation, the state becomes  $|\psi'\rangle = D(R)|\psi\rangle$ . The eigenvalue of operator  $V$  can be expressed as follows:

$$\langle \psi' | V | \psi' \rangle = \langle \psi | D(R)^\dagger V D(R) | \psi \rangle = \langle \psi | V | \psi \rangle \quad (56)$$

Equation (56) is true for all  $\psi$  so that  $V = D(R)^\dagger V D(R)$  [22]. In specific case,  $D(R) = 1 - \frac{i\epsilon \mathbf{J} \cdot \hat{\mathbf{n}}}{\hbar}$ , where  $\hat{\mathbf{n}}$  is the rotating axis;  $\mathbf{J}$  is the angular momentum of this system;  $\epsilon$  is the small rotating angle. After neglecting the higher term of  $\epsilon$ , the equation (56) becomes:

$$\left(1 + \frac{i\epsilon \mathbf{J} \cdot \hat{\mathbf{n}}}{\hbar}\right) V \left(1 - \frac{i\epsilon \mathbf{J} \cdot \hat{\mathbf{n}}}{\hbar}\right) = V + \frac{i\epsilon}{\hbar} [V, \mathbf{J} \cdot \hat{\mathbf{n}}] = V \quad (57)$$

We get  $[V, \mathbf{J} \cdot \hat{\mathbf{n}}] = 0$ . If it is true for all  $\hat{\mathbf{n}}$ , then  $V$  must commute with  $\mathbf{J}$ .

## vector operator

If an operator  $\mathbf{V}$  is a vector operator, its expectation value must satisfy  $V_i = \sum_j R_{ij} V_j$ , where  $R_{ij}$  is the rotating matrix. Then the equation (57) becomes:

$$V_i + \frac{i\epsilon}{\hbar} [V_i, \mathbf{J} \cdot \hat{\mathbf{n}}] = \sum_j R_{ij}(n; \epsilon) V_j \quad (58)$$

For  $n$  in  $z$ -axis, we get the rotating matrix:

$$R(n; \epsilon) = \begin{pmatrix} 1 & -\epsilon & 0 \\ \epsilon & 1 & 0 \\ 0 & 0 & 1 \end{pmatrix} \quad (59)$$

We choose  $i = 1, 2, 3$  and then we can get the commutation relation:

$$[V_i, J_j] = i\hbar \epsilon_{ijk} V_k \quad (60)$$

Therefore, If the operator  $\mathbf{V}$  satisfy equation (60), we can say that  $\mathbf{V}$  is a vector operator.

## tensor operator

we can use two vector operator to structure a tensor operator, like  $T_{ij} = \mathbf{U}_i \mathbf{V}_j$ , and we will get nine components. We can also write  $T_{ij}$  as follows:

$$U_i V_j = \frac{\mathbf{U} \cdot \mathbf{V}}{3} \delta_{ij} + \frac{\epsilon_{ijk} (\mathbf{U} \times \mathbf{V})_k}{2} + \left( \frac{U_i V_j + U_j V_i}{2} - \frac{\mathbf{U} \cdot \mathbf{V}}{3} \delta_{ij} \right) \quad (61)$$

The first term is the scalar product invariant under rotation. The second term is an anti-symmetric tensor. The last term is a  $3 \times 3$  traceless tensor with 5 components. The definition of tensor operator:

$$D(R) T_q^{(k)} D^\dagger(R) = \sum_{q'=-k}^k D_{q'q}^{(k)}(R) T_{q'}^{(k)} \quad (62)$$

we take equation (62) into the equation (57) and we get:

$$[\mathbf{J} \cdot \hat{\mathbf{n}}, T_q^{(k)}] = \sum_{q'=-k}^k T_{q'}^{(k)} \langle kq' | \mathbf{J} \cdot \hat{\mathbf{n}} | kq \rangle \quad (63)$$

## Appendix C: SO(3) generator

For the rotation symmetry (SO(3) group), we have the relation:

$$[J_i, J_j] = i\epsilon_{ijk} J_k \quad (64)$$

where  $J_i, J_j, J_k$  is the generator of SO(3). If we need SO(4), we will have 6 generators. We can separate six generators into two groups. One is  $J_1, J_2, J_3$  which is the same as that in the SO(3) group and another is  $L_1, L_2, L_3$ . They have the relation as follows:

$$\begin{aligned} [J_i, J_j] &= i\epsilon_{ijk} J_k \\ [J_i, L_j] &= i\epsilon_{ijk} L_k \\ [L_i, L_j] &= i\epsilon_{ijk} J_k \end{aligned} \quad (65)$$

We can mix those six generators as:  $J_{+,i} = \frac{J_i + L_i}{2}$ ;  $J_{-,i} = \frac{J_i - L_i}{2}$ , then the relation becomes:

$$\begin{aligned} [J_{+,i}, J_{+,j}] &= i\epsilon_{ijk} J_{+,k} \\ [J_{-,i}, J_{-,j}] &= i\epsilon_{ijk} J_{-,k} \\ [J_{+,i}, J_{-,j}] &= 0 \end{aligned} \quad (66)$$

We now have two separate SO(3), which means  $SO(4) = SO(3) \otimes SO(3)$ .

**Appendix D: 1D spin model Hamiltonian for 5 sites as an example**

Table 5: This table shows the nonzero value of 1D spin model Hamiltonian(32\*32 matrix)for 5 sites in the original basis as an example.The subscript denotes rows and columns of Hamiltonian.

$H_{row,column}$	Value	$H_{row,column}$	Value	$H_{row,column}$	Value
$H_{1,1}$	$(5*\lambda_2)/4$	$H_{1,4}$	$(1 - \lambda_1)/4$	$H_{1,7}$	$(1 - \lambda_1)/4$
$H_{1,13}$	$(1 - \lambda_1)/4$	$H_{1,18}$	$(1 - \lambda_1)/4$	$H_{1,25}$	$(1 - \lambda_1)/4$
$H_{2,2}$	$\lambda_2/4$	$H_{2,3}$	$(1 + \lambda_1)/4$	$H_{2,8}$	$(1 - \lambda_1)/4$
$H_{2,14}$	$(1 - \lambda_1)/4$	$H_{2,17}$	$(1 + \lambda_1)/4$	$H_{2,26}$	$(1 - \lambda_1)/4$
$H_{3,2}$	$(1 + \lambda_1)/4$	$H_{3,3}$	$\lambda_2/4$	$H_{3,5}$	$(1 + \lambda_1)/4$
$H_{3,15}$	$(1 - \lambda_1)/4$	$H_{3,20}$	$(1 - \lambda_1)/4$	$H_{3,27}$	$(1 - \lambda_1)/4$
$H_{4,1}$	$(1 - \lambda_1)/4$	$H_{4,4}$	$\lambda_2/4$	$H_{4,6}$	$(1 + \lambda_1)/4$
$H_{4,16}$	$(1 - \lambda_1)/4$	$H_{4,19}$	$(1 + \lambda_1)/4$	$H_{4,28}$	$(1 - \lambda_1)/4$
$H_{5,3}$	$(1 + \lambda_1)/4$	$H_{5,5}$	$\lambda_2/4$	$H_{5,8}$	$(1 - \lambda_1)/4$
$H_{5,9}$	$(1 + \lambda_1)/4$	$H_{5,22}$	$(1 - \lambda_1)/4$	$H_{5,29}$	$(1 - \lambda_1)/4$
$H_{6,4}$	$(1 + \lambda_1)/4$	$H_{6,6}$	$(-3*\lambda_2)/4$	$H_{6,7}$	$(1 + \lambda_1)/4$
$H_{6,10}$	$(1 + \lambda_1)/4$	$H_{6,21}$	$(1 + \lambda_1)/4$	$H_{6,30}$	$(1 - \lambda_1)/4$
$H_{7,1}$	$(1 - \lambda_1)/4$	$H_{7,6}$	$(1 + \lambda_1)/4$	$H_{7,7}$	$\lambda_2/4$
$H_{7,11}$	$(1 + \lambda_1)/4$	$H_{7,24}$	$(1 - \lambda_1)/4$	$H_{7,31}$	$(1 - \lambda_1)/4$
$H_{8,2}$	$(1 - \lambda_1)/4$	$H_{8,5}$	$(1 - \lambda_1)/4$	$H_{8,8}$	$\lambda_2/4$
$H_{8,12}$	$(1 + \lambda_1)/4$	$H_{8,23}$	$(1 + \lambda_1)/4$	$H_{8,32}$	$(1 - \lambda_1)/4$
$H_{9,5}$	$(1 + \lambda_1)/4$	$H_{9,9}$	$\lambda_2/4$	$H_{9,12}$	$(1 - \lambda_1)/4$
$H_{9,15}$	$(1 - \lambda_1)/4$	$H_{9,17}$	$(1 + \lambda_1)/4$	$H_{9,26}$	$(1 - \lambda_1)/4$
$H_{10,6}$	$(1 + \lambda_1)/4$	$H_{10,10}$	$(-3*\lambda_2)/4$	$H_{10,11}$	$(1 + \lambda_1)/4$
$H_{10,16}$	$(1 - \lambda_1)/4$	$H_{10,18}$	$(1 + \lambda_1)/4$	$H_{10,25}$	$(1 + \lambda_1)/4$
$H_{11,7}$	$(1 + \lambda_1)/4$	$H_{11,10}$	$(1 + \lambda_1)/4$	$H_{11,11}$	$(-3*\lambda_2)/4$
$H_{11,13}$	$(1 + \lambda_1)/4$	$H_{11,19}$	$(1 + \lambda_1)/4$	$H_{11,28}$	$(1 - \lambda_1)/4$
$H_{12,8}$	$(1 + \lambda_1)/4$	$H_{12,9}$	$(1 - \lambda_1)/4$	$H_{12,12}$	$(-3*\lambda_2)/4$
$H_{12,14}$	$(1 + \lambda_1)/4$	$H_{12,20}$	$(1 + \lambda_1)/4$	$H_{12,27}$	$(1 + \lambda_1)/4$
$H_{13,1}$	$(1 - \lambda_1)/4$	$H_{13,11}$	$(1 + \lambda_1)/4$	$H_{13,13}$	$\lambda_2/4$
$H_{13,16}$	$(1 - \lambda_1)/4$	$H_{13,21}$	$(1 + \lambda_1)/4$	$H_{13,30}$	$(1 - \lambda_1)/4$
$H_{14,2}$	$(1 - \lambda_1)/4$	$H_{14,12}$	$(1 + \lambda_1)/4$	$H_{14,14}$	$(-3*\lambda_2)/4$
$H_{14,15}$	$(1 + \lambda_1)/4$	$H_{14,22}$	$(1 + \lambda_1)/4$	$H_{14,29}$	$(1 + \lambda_1)/4$
$H_{15,3}$	$(1 - \lambda_1)/4$	$H_{15,9}$	$(1 - \lambda_1)/4$	$H_{15,14}$	$(1 + \lambda_1)/4$
$H_{15,15}$	$\lambda_2/4$	$H_{15,23}$	$(1 + \lambda_1)/4$	$H_{15,32}$	$(1 - \lambda_1)/4$
$H_{16,4}$	$(1 - \lambda_1)/4$	$H_{16,10}$	$(1 - \lambda_1)/4$	$H_{16,13}$	$(1 - \lambda_1)/4$
$H_{16,16}$	$\lambda_2/4$	$H_{16,24}$	$(1 + \lambda_1)/4$	$H_{16,31}$	$(1 + \lambda_1)/4$
$H_{17,2}$	$(1 + \lambda_1)/4$	$H_{17,9}$	$(1 + \lambda_1)/4$	$H_{17,17}$	$\lambda_2/4$
$H_{17,20}$	$(1 - \lambda_1)/4$	$H_{17,23}$	$(1 - \lambda_1)/4$	$H_{17,29}$	$(1 - \lambda_1)/4$
$H_{18,1}$	$(1 - \lambda_1)/4$	$H_{18,10}$	$(1 + \lambda_1)/4$	$H_{18,18}$	$\lambda_2/4$
$H_{18,19}$	$(1 + \lambda_1)/4$	$H_{18,24}$	$(1 - \lambda_1)/4$	$H_{18,30}$	$(1 - \lambda_1)/4$
$H_{19,4}$	$(1 + \lambda_1)/4$	$H_{19,11}$	$(1 + \lambda_1)/4$	$H_{19,18}$	$(1 + \lambda_1)/4$
$H_{19,19}$	$(-3*\lambda_2)/4$	$H_{19,21}$	$(1 + \lambda_1)/4$	$H_{19,31}$	$(1 - \lambda_1)/4$
$H_{20,3}$	$(1 - \lambda_1)/4$	$H_{20,12}$	$(1 + \lambda_1)/4$	$H_{20,17}$	$(1 - \lambda_1)/4$
$H_{20,20}$	$\lambda_2/4$	$H_{20,22}$	$(1 + \lambda_1)/4$	$H_{20,32}$	$(1 - \lambda_1)/4$
$H_{21,6}$	$(1 + \lambda_1)/4$	$H_{21,13}$	$(1 + \lambda_1)/4$	$H_{21,19}$	$(1 + \lambda_1)/4$
$H_{21,21}$	$(-3*\lambda_2)/4$	$H_{21,24}$	$(1 - \lambda_1)/4$	$H_{21,25}$	$(1 + \lambda_1)/4$
$H_{22,5}$	$(1 - \lambda_1)/4$	$H_{22,14}$	$(1 + \lambda_1)/4$	$H_{22,20}$	$(1 + \lambda_1)/4$
$H_{22,22}$	$(-3*\lambda_2)/4$	$H_{22,23}$	$(1 + \lambda_1)/4$	$H_{22,26}$	$(1 + \lambda_1)/4$
$H_{23,8}$	$(1 + \lambda_1)/4$	$H_{23,15}$	$(1 + \lambda_1)/4$	$H_{23,17}$	$(1 - \lambda_1)/4$
$H_{23,22}$	$(1 + \lambda_1)/4$	$H_{23,23}$	$(-3*\lambda_2)/4$	$H_{23,27}$	$(1 + \lambda_1)/4$
$H_{24,7}$	$(1 - \lambda_1)/4$	$H_{24,16}$	$(1 + \lambda_1)/4$	$H_{24,18}$	$(1 - \lambda_1)/4$
$H_{24,21}$	$(1 - \lambda_1)/4$	$H_{24,24}$	$\lambda_2/4$	$H_{24,28}$	$(1 + \lambda_1)/4$
$H_{25,1}$	$(1 - \lambda_1)/4$	$H_{25,10}$	$(1 + \lambda_1)/4$	$H_{25,21}$	$(1 + \lambda_1)/4$
$H_{25,25}$	$\lambda_2/4$	$H_{25,28}$	$(1 - \lambda_1)/4$	$H_{25,31}$	$(1 - \lambda_1)/4$
$H_{26,2}$	$(1 - \lambda_1)/4$	$H_{26,9}$	$(1 - \lambda_1)/4$	$H_{26,22}$	$(1 + \lambda_1)/4$

$H_{row,column}$	Value	$H_{row,column}$	Value	$H_{row,column}$	Value
$H_{26,26}$	$\lambda_2/4$	$H_{26,27}$	$(1 + \lambda_1)/4$	$H_{26,32}$	$(1 - \lambda_1)/4$
$H_{27,3}$	$(1 - \lambda_1)/4$	$H_{27,12}$	$(1 + \lambda_1)/4$	$H_{27,23}$	$(1 + \lambda_1)/4$
$H_{27,26}$	$(1 + \lambda_1)/4$	$H_{27,27}$	$(-3*\lambda_2)/4$	$H_{27,29}$	$(1 + \lambda_1)/4$
$H_{28,4}$	$(1 - \lambda_1)/4$	$H_{28,11}$	$(1 - \lambda_1)/4$	$H_{28,24}$	$(1 + \lambda_1)/4$
$H_{28,25}$	$(1 - \lambda_1)/4$	$H_{28,28}$	$\lambda_2/4$	$H_{28,30}$	$(1 + \lambda_1)/4$
$H_{29,5}$	$(1 - \lambda_1)/4$	$H_{29,14}$	$(1 + \lambda_1)/4$	$H_{29,17}$	$(1 - \lambda_1)/4$
$H_{29,27}$	$(1 + \lambda_1)/4$	$H_{29,29}$	$\lambda_2/4$	$H_{29,32}$	$(1 - \lambda_1)/4$
$H_{30,6}$	$(1 - \lambda_1)/4$	$H_{30,13}$	$(1 - \lambda_1)/4$	$H_{30,18}$	$(1 - \lambda_1)/4$
$H_{30,28}$	$(1 + \lambda_1)/4$	$H_{30,30}$	$\lambda_2/4$	$H_{30,31}$	$(1 + \lambda_1)/4$
$H_{31,7}$	$(1 - \lambda_1)/4$	$H_{31,16}$	$(1 + \lambda_1)/4$	$H_{31,19}$	$(1 - \lambda_1)/4$
$H_{31,25}$	$(1 - \lambda_1)/4$	$H_{31,30}$	$(1 + \lambda_1)/4$	$H_{31,31}$	$\lambda_2/4$
$H_{32,8}$	$(1 - \lambda_1)/4$	$H_{32,15}$	$(1 - \lambda_1)/4$	$H_{32,20}$	$(1 - \lambda_1)/4$
$H_{32,26}$	$(1 - \lambda_1)/4$	$H_{32,29}$	$(1 - \lambda_1)/4$	$H_{32,32}$	$(5*\lambda_2)/4$

Table 6: This table shows the Hamiltonian after using spin flip operator

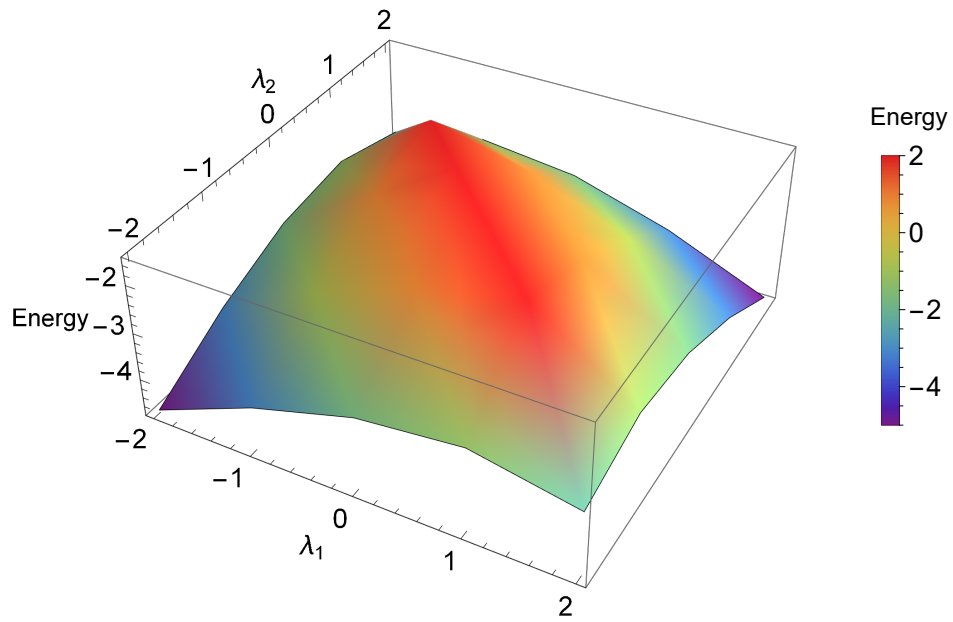
$H_{row,column}$	Value	$H_{row,column}$	Value	$H_{row,column}$	Value
$H_{1,1}$	$(5*\lambda_2)/4$	$H_{1,4}$	$(1 - \lambda_1)/4$	$H_{1,7}$	$(1 - \lambda_1)/4$
$H_{1,13}$	$(1 - \lambda_1)/4$	$H_{1,18}$	$(1 - \lambda_1)/4$	$H_{1,25}$	$(1 - \lambda_1)/4$
$H_{2,2}$	$\lambda_2/4$	$H_{2,3}$	$(1 + \lambda_1)/4$	$H_{2,8}$	$(1 - \lambda_1)/4$
$H_{2,14}$	$(1 - \lambda_1)/4$	$H_{2,17}$	$(1 + \lambda_1)/4$	$H_{2,26}$	$(1 - \lambda_1)/4$
$H_{3,2}$	$(1 + \lambda_1)/4$	$H_{3,3}$	$\lambda_2/4$	$H_{3,5}$	$(1 + \lambda_1)/4$
$H_{3,15}$	$(1 - \lambda_1)/4$	$H_{3,20}$	$(1 - \lambda_1)/4$	$H_{3,27}$	$(1 - \lambda_1)/4$
$H_{4,1}$	$(1 - \lambda_1)/4$	$H_{4,4}$	$\lambda_2/4$	$H_{4,6}$	$(1 + \lambda_1)/4$
$H_{4,16}$	$(1 - \lambda_1)/4$	$H_{4,19}$	$(1 + \lambda_1)/4$	$H_{4,28}$	$(1 - \lambda_1)/4$
$H_{5,3}$	$(1 + \lambda_1)/4$	$H_{5,5}$	$\lambda_2/4$	$H_{5,8}$	$(1 - \lambda_1)/4$
$H_{5,9}$	$(1 + \lambda_1)/4$	$H_{5,22}$	$(1 - \lambda_1)/4$	$H_{5,29}$	$(1 - \lambda_1)/4$
$H_{6,4}$	$(1 + \lambda_1)/4$	$H_{6,6}$	$(-3*\lambda_2)/4$	$H_{6,7}$	$(1 + \lambda_1)/4$
$H_{6,10}$	$(1 + \lambda_1)/4$	$H_{6,21}$	$(1 + \lambda_1)/4$	$H_{6,30}$	$(1 - \lambda_1)/4$
$H_{7,1}$	$(1 - \lambda_1)/4$	$H_{7,6}$	$(1 + \lambda_1)/4$	$H_{7,7}$	$\lambda_2/4$
$H_{7,11}$	$(1 + \lambda_1)/4$	$H_{7,24}$	$(1 - \lambda_1)/4$	$H_{7,31}$	$(1 - \lambda_1)/4$
$H_{8,2}$	$(1 - \lambda_1)/4$	$H_{8,5}$	$(1 - \lambda_1)/4$	$H_{8,8}$	$\lambda_2/4$
$H_{8,12}$	$(1 + \lambda_1)/4$	$H_{8,23}$	$(1 + \lambda_1)/4$	$H_{8,32}$	$(1 - \lambda_1)/4$
$H_{9,5}$	$(1 + \lambda_1)/4$	$H_{9,9}$	$\lambda_2/4$	$H_{9,12}$	$(1 - \lambda_1)/4$
$H_{9,15}$	$(1 - \lambda_1)/4$	$H_{9,17}$	$(1 + \lambda_1)/4$	$H_{9,26}$	$(1 - \lambda_1)/4$
$H_{10,6}$	$(1 + \lambda_1)/4$	$H_{10,10}$	$(-3*\lambda_2)/4$	$H_{10,11}$	$(1 + \lambda_1)/4$
$H_{10,16}$	$(1 - \lambda_1)/4$	$H_{10,18}$	$(1 + \lambda_1)/4$	$H_{10,25}$	$(1 + \lambda_1)/4$
$H_{11,7}$	$(1 + \lambda_1)/4$	$H_{11,10}$	$(1 + \lambda_1)/4$	$H_{11,11}$	$(-3*\lambda_2)/4$
$H_{11,13}$	$(1 + \lambda_1)/4$	$H_{11,19}$	$(1 + \lambda_1)/4$	$H_{11,28}$	$(1 - \lambda_1)/4$
$H_{12,8}$	$(1 + \lambda_1)/4$	$H_{12,9}$	$(1 - \lambda_1)/4$	$H_{12,12}$	$(-3*\lambda_2)/4$
$H_{12,14}$	$(1 + \lambda_1)/4$	$H_{12,20}$	$(1 + \lambda_1)/4$	$H_{12,27}$	$(1 + \lambda_1)/4$
$H_{13,1}$	$(1 - \lambda_1)/4$	$H_{13,11}$	$(1 + \lambda_1)/4$	$H_{13,13}$	$\lambda_2/4$
$H_{13,16}$	$(1 - \lambda_1)/4$	$H_{13,21}$	$(1 + \lambda_1)/4$	$H_{13,30}$	$(1 - \lambda_1)/4$
$H_{14,2}$	$(1 - \lambda_1)/4$	$H_{14,12}$	$(1 + \lambda_1)/4$	$H_{14,14}$	$(-3*\lambda_2)/4$
$H_{14,15}$	$(1 + \lambda_1)/4$	$H_{14,22}$	$(1 + \lambda_1)/4$	$H_{14,29}$	$(1 + \lambda_1)/4$
$H_{15,3}$	$(1 - \lambda_1)/4$	$H_{15,9}$	$(1 - \lambda_1)/4$	$H_{15,14}$	$(1 + \lambda_1)/4$
$H_{15,15}$	$\lambda_2/4$	$H_{15,23}$	$(1 + \lambda_1)/4$	$H_{15,32}$	$(1 - \lambda_1)/4$
$H_{16,4}$	$(1 - \lambda_1)/4$	$H_{16,10}$	$(1 - \lambda_1)/4$	$H_{16,13}$	$(1 - \lambda_1)/4$
$H_{16,16}$	$\lambda_2/4$	$H_{16,24}$	$(1 + \lambda_1)/4$	$H_{16,31}$	$(1 + \lambda_1)/4$
$H_{17,2}$	$(1 + \lambda_1)/4$	$H_{17,9}$	$(1 + \lambda_1)/4$	$H_{17,17}$	$\lambda_2/4$
$H_{17,20}$	$(1 - \lambda_1)/4$	$H_{17,23}$	$(1 - \lambda_1)/4$	$H_{17,29}$	$(1 - \lambda_1)/4$
$H_{18,1}$	$(1 - \lambda_1)/4$	$H_{18,10}$	$(1 + \lambda_1)/4$	$H_{18,18}$	$\lambda_2/4$
$H_{18,19}$	$(1 + \lambda_1)/4$	$H_{18,24}$	$(1 - \lambda_1)/4$	$H_{18,30}$	$(1 - \lambda_1)/4$
$H_{19,4}$	$(1 + \lambda_1)/4$	$H_{19,11}$	$(1 + \lambda_1)/4$	$H_{19,18}$	$(1 + \lambda_1)/4$
$H_{19,19}$	$(-3*\lambda_2)/4$	$H_{19,21}$	$(1 + \lambda_1)/4$	$H_{19,31}$	$(1 - \lambda_1)/4$
$H_{20,3}$	$(1 - \lambda_1)/4$	$H_{20,12}$	$(1 + \lambda_1)/4$	$H_{20,17}$	$(1 - \lambda_1)/4$

$H_{row,column}$	Value	$H_{row,column}$	Value	$H_{row,column}$	Value
$H_{20,20}$	$\lambda_2/4$	$H_{20,22}$	$(1 + \lambda_1)/4$	$H_{20,32}$	$(1 - \lambda_1)/4$
$H_{21,6}$	$(1 + \lambda_1)/4$	$H_{21,13}$	$(1 + \lambda_1)/4$	$H_{21,19}$	$(1 + \lambda_1)/4$
$H_{21,21}$	$(-3*\lambda_2)/4$	$H_{21,24}$	$(1 - \lambda_1)/4$	$H_{21,25}$	$(1 + \lambda_1)/4$
$H_{22,5}$	$(1 - \lambda_1)/4$	$H_{22,14}$	$(1 + \lambda_1)/4$	$H_{22,20}$	$(1 + \lambda_1)/4$
$H_{22,22}$	$(-3*\lambda_2)/4$	$H_{22,23}$	$(1 + \lambda_1)/4$	$H_{22,26}$	$(1 + \lambda_1)/4$
$H_{23,8}$	$(1 + \lambda_1)/4$	$H_{23,15}$	$(1 + \lambda_1)/4$	$H_{23,17}$	$(1 - \lambda_1)/4$
$H_{23,22}$	$(1 + \lambda_1)/4$	$H_{23,23}$	$(-3*\lambda_2)/4$	$H_{23,27}$	$(1 + \lambda_1)/4$
$H_{24,7}$	$(1 - \lambda_1)/4$	$H_{24,16}$	$(1 + \lambda_1)/4$	$H_{24,18}$	$(1 - \lambda_1)/4$
$H_{24,21}$	$(1 - \lambda_1)/4$	$H_{24,24}$	$\lambda_2/4$	$H_{24,28}$	$(1 + \lambda_1)/4$
$H_{25,1}$	$(1 - \lambda_1)/4$	$H_{25,10}$	$(1 + \lambda_1)/4$	$H_{25,21}$	$(1 + \lambda_1)/4$
$H_{25,25}$	$\lambda_2/4$	$H_{25,28}$	$(1 - \lambda_1)/4$	$H_{25,31}$	$(1 - \lambda_1)/4$
$H_{26,2}$	$(1 - \lambda_1)/4$	$H_{26,9}$	$(1 - \lambda_1)/4$	$H_{26,22}$	$(1 + \lambda_1)/4$
$H_{26,26}$	$\lambda_2/4$	$H_{26,27}$	$(1 + \lambda_1)/4$	$H_{26,32}$	$(1 - \lambda_1)/4$
$H_{27,3}$	$(1 - \lambda_1)/4$	$H_{27,12}$	$(1 + \lambda_1)/4$	$H_{27,23}$	$(1 + \lambda_1)/4$
$H_{27,26}$	$(1 + \lambda_1)/4$	$H_{27,27}$	$(-3*\lambda_2)/4$	$H_{27,29}$	$(1 + \lambda_1)/4$
$H_{28,4}$	$(1 - \lambda_1)/4$	$H_{28,11}$	$(1 - \lambda_1)/4$	$H_{28,24}$	$(1 + \lambda_1)/4$
$H_{28,25}$	$(1 - \lambda_1)/4$	$H_{28,28}$	$\lambda_2/4$	$H_{28,30}$	$(1 + \lambda_1)/4$
$H_{29,5}$	$(1 - \lambda_1)/4$	$H_{29,14}$	$(1 + \lambda_1)/4$	$H_{29,17}$	$(1 - \lambda_1)/4$
$H_{29,27}$	$(1 + \lambda_1)/4$	$H_{29,29}$	$\lambda_2/4$	$H_{29,32}$	$(1 - \lambda_1)/4$
$H_{30,6}$	$(1 - \lambda_1)/4$	$H_{30,13}$	$(1 - \lambda_1)/4$	$H_{30,18}$	$(1 - \lambda_1)/4$
$H_{30,28}$	$(1 + \lambda_1)/4$	$H_{30,30}$	$\lambda_2/4$	$H_{30,31}$	$(1 + \lambda_1)/4$
$H_{31,7}$	$(1 - \lambda_1)/4$	$H_{31,16}$	$(1 + \lambda_1)/4$	$H_{31,19}$	$(1 - \lambda_1)/4$
$H_{31,25}$	$(1 - \lambda_1)/4$	$H_{31,30}$	$(1 + \lambda_1)/4$	$H_{31,31}$	$\lambda_2/4$
$H_{32,8}$	$(1 - \lambda_1)/4$	$H_{32,15}$	$(1 - \lambda_1)/4$	$H_{32,20}$	$(1 - \lambda_1)/4$
$H_{32,26}$	$(1 - \lambda_1)/4$	$H_{32,29}$	$(1 - \lambda_1)/4$	$H_{32,32}$	$(5*\lambda_2)/4$

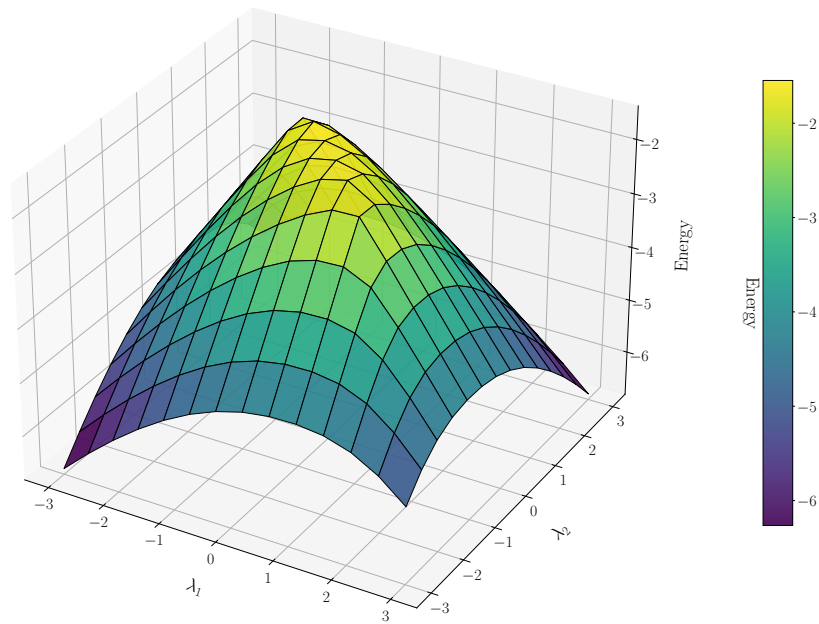
In the table 5 and 6, we can clear see that after using spin flip operator, the Hamiltonian is block diagonalized because  $H_{1\sim 16,17\sim 32} = 0$  and  $H_{17\sim 32,1\sim 16} = 0$ .

### Appendix E: Ground energy of 1D spin model for 6 sites

For 6 sites Heisenberg model,in the paper,we use symmetry operators to get the ground state.Therefore, we want to know the correctness of this method.We plot the ground 3D pictures in the figure19.



(a) theoretical ground energy



(b) ground energy using [15]

Figure 19: 6 sites Heisenberg model ground energy 3D figure

We also plot energy versus  $\lambda_2$  in the figure 20.

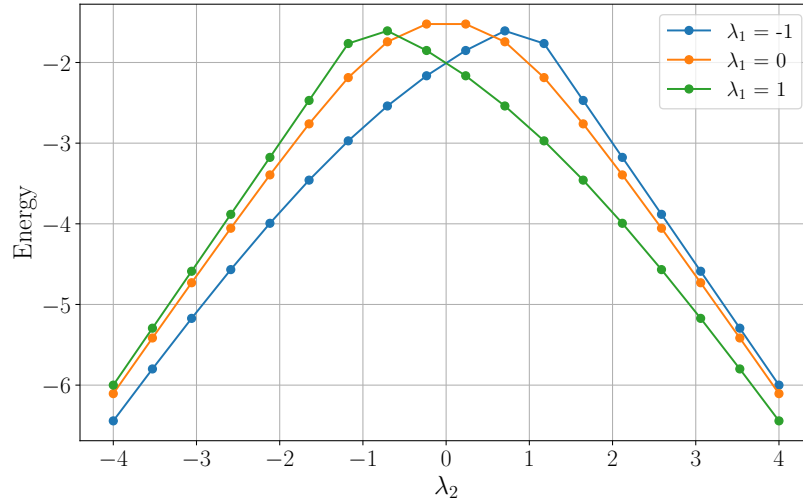


Figure 20: The dot plot is theoretical results for 6 sites and the curve is results for 6 sites using package[15]. We can see that curves perfectly link points.

We can conclude that by using block diagonalization, we can still get the right answer.

### Appendix F: Basis construction of 1D Bose-Hubbard model

We need to arrange  $N_b$  bosonic particles into  $L$  sites. Since the particles are bosons, there is no restriction on the number of particles per site. The total number of possible arrangements is given by  $\frac{(N_b+L-1)!}{(L-1)!N_b!}$ , which can be derived using combinatorial methods. For example, to arrange 2 particles in 3 sites, the possible arrangements are: (2,0,0) (1,1,0), (1,0,1),(0,2,0), (0,1,1), and (0,0,2). We use these orthonormal basis states to construct the Hamiltonian in the figure 21.

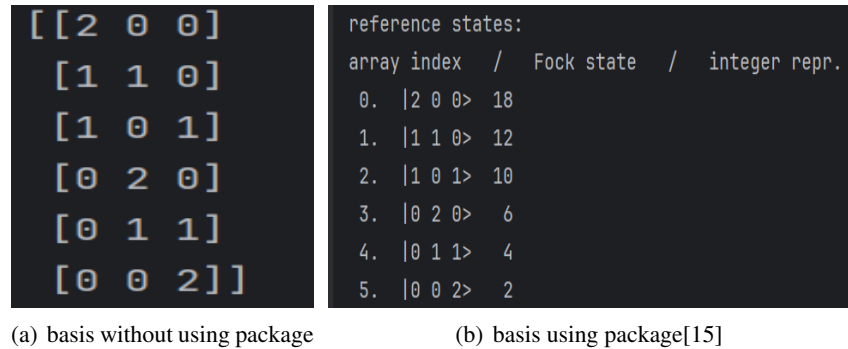


Figure 21: We use two different approaches to construct basis when  $L=3, N_b=2$

After we get the basis, we can construct the Hamiltonian to get the ground energy of this system.

### Appendix G: Detailed derivation of Gutzwiller Hamiltonian

We take the Gutzwiller wavefunction with  $f_n = (1 - 2\alpha^2)^{1/2}, f_{n-1} = f_{n+1} = \alpha$ . We can expand the hopping energy to the second order.

$$H_t = -2t\alpha^2|\sqrt{n} + \sqrt{n+1}|^2 \approx -8tn\alpha^2 \tag{67}$$

Moreover, the  $n$  is large enough so that we can use the approximation. If we apply  $\mu = U(n - \frac{1}{2})$  into the chemical and potential term, the relation becomes

$$H_U + H_\mu = U\alpha^2 - \frac{U}{2}n^2 \tag{68}$$

where  $\alpha$  is a small parameter, just like the order parameter in the mean field. In the Landau theory, the phase transition occurs when

$$U = 8nt \quad (69)$$

Mathematically, there is no significant difference between the Gutzwiller variational ansatz and the mean-field approximation when the number of particles  $n$  is sufficiently large in three dimensions. However, in one dimension, the Gutzwiller variational ansatz provides a more concrete and detailed description compared to the mean-field approach.

## Appendix H: Detailed derivation of Mean field Hamiltonian

From eq(33) and eq(34), we only need to calculate  $A(n_b)$ . By using equation  $\hat{b}_j |n_b\rangle = \sqrt{n_b} |n_b - 1\rangle$  and  $\hat{b}_j^\dagger |n_b\rangle = \sqrt{n_b + 1} |n_b + 1\rangle$ , we can easily get the second perturbation term:

$$\begin{aligned} E'(n_b) &= E(n_b) + \frac{(-2tb_0\sqrt{n_b+1})^2}{E(n_b) - E(n_b+1)} + \frac{(-2tb_0\sqrt{n_b})^2}{E(n_b) - E(n_b-1)} \\ &= E(n_b) + (2tb_0)^2 \left[ \frac{n_b+1}{\mu - Un_b} + \frac{n_b}{U(n_b-1) - \mu} \right] \end{aligned} \quad (70)$$

After we apply the constant energy  $2tb_0^2$ , the average energy per site is

$$E' = E(n_b) + \{(2t)^2 \left[ \frac{n_b+1}{\mu - Un_b} + \frac{n_b}{U(n_b-1) - \mu} \right] + 2t\} b_0^2 \quad (71)$$

As we discuss above, phase transition occurs when the coefficient is 0, which means

$$2t \left( \frac{n_b}{U(n_b-1) - \mu} + \frac{n_b+1}{\mu - Un_b} \right) = -1 \quad (72)$$

If we unitize  $t$  and  $\mu: \omega = \frac{2t}{U}$  and  $\mu' = \frac{\mu}{U}$ , we can get the function between  $\omega$  and  $\mu'$  when given  $n_b$ . The equation(22) becomes:

$$\left(\frac{\mu}{U}\right)^2 - (2n_b - 1 - \frac{2t}{U}) \frac{\mu}{U} + \frac{2t}{U} + n_b(n_b - 1) = 0 \quad (73)$$

Solving this quadratic equation, we get

$$\left(\frac{\mu}{U}\right)_\pm = n_b - \frac{1}{2} - \frac{t}{U} \pm \sqrt{\left(\frac{t}{U}\right)^2 - (1 - 2n_b) \frac{t}{U} + \frac{1}{4}} \quad (74)$$

Moreover, in order to plot pictures more easily, we can rewrite equation 23 like

$$\frac{t}{U} = \frac{(n_b - \frac{\mu}{U})(\frac{\mu}{U} + 1 - n_b)}{2(\frac{\mu}{U} + 1)} \quad (75)$$

The wave function becomes:

$$|n'_b\rangle = |n_b\rangle - 2tb_0 \frac{\sqrt{n_b+1}}{\mu - Un_b} - 2tb_0 \frac{\sqrt{n_b}}{U(n_b-1) - \mu} \quad (76)$$

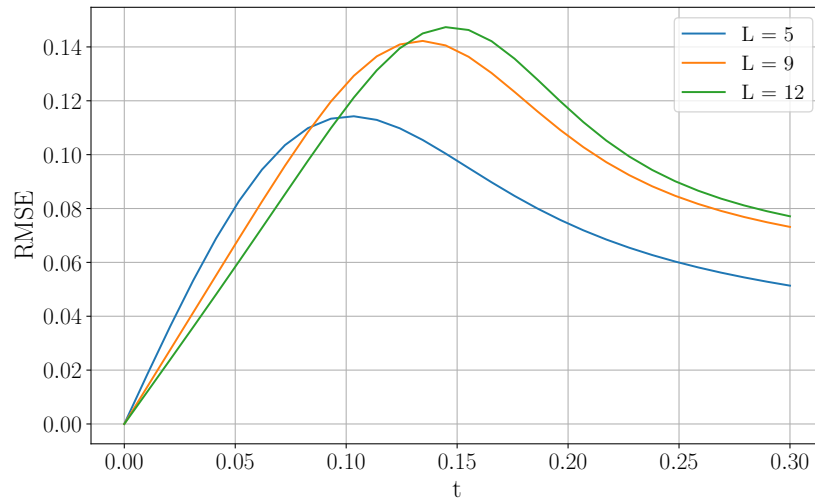
**Appendix I: correlation function for different sizes**

Figure 22: residual vs t for different sizes[15]

As the number of sites increases, the peak values of the transition point become nearly constant. in the figure 22. This suggests that the transition point approaches the value representative of the true physical system.